nature

https://doi.org/10.1038/s41586-022-05053-w

Accelerated Article Preview

Antibody evasion by SARS-CoV-2 Omicron subvariants BA.2.12.1, BA.4, & BA.5

Received: 26 May 2022

Accepted: 30 June 2022

Accelerated Article Preview
Published online: 05 July 2022

Cite this article as: Wang, Q. et al. Antibody evasion by SARS-CoV-2 Omicron subvariants BA.2.12.1, BA.4, & BA.5. *Nature* https://doi.org/10.1038/s41586-022-05053-w (2022).

Qian Wang, Yicheng Guo, Sho Iketani, Manoj S. Nair, Zhiteng Li, Hiroshi Mohri, Maple Wang, Jian Yu, Anthony D. Bowen, Jennifer Y. Chang, Jayesh G. Shah, Nadia Nguyen, Zhiwei Chen, Kathrine Meyers, Michael T. Yin, Magdalena E. Sobieszczyk, Zizhang Sheng, Yaoxing Huang, Lihong Liu & David D. Ho

Antibody evasion by SARS-CoV-2 Omicron subvariants BA.2.12.1, BA.4, & BA.5

Qian Wang[1*], Yicheng Guo[1*], Sho Iketani[1,2], Manoj S. Nair[1], Zhiteng Li[1], Hiroshi Mohri[1], Maple Wang[1], Jian Yu[1], Anthony D. Bowen[1,3], Jennifer Y. Chang[3], Jayesh G. Shah[3], Nadia Nguyen[1], Zhiwei Chen[4], Kathrine Meyers[1,3], Michael T. Yin[1,3], Magdalena E. Sobieszczyk[1,3], Zizhang Sheng[1], Yaoxing Huang[1], Lihong Liu[1#], and David D. Ho[1,2,3#]

[1]Aaron Diamond AIDS Research Center, Columbia University Vagelos College of Physicians and Surgeons, New York, NY, USA.

[2]Department of Microbiology and Immunology, Columbia University Vagelos College of Physicians and Surgeons, New York, NY, USA.

[3]Division of Infectious Diseases, Department of Medicine, Columbia University Vagelos College of Physicians and Surgeons, New York, NY, USA.

[4]AIDS Institute and Department of Microbiology, Li Ka Shing Faculty of Medicine, The University of Hong Kong, Pokfulam, Hong Kong Special Administrative Region, People's Republic of China.

*Equal contribution

[#]Address correspondence to Lihong Liu (ll3411@cumc.columbia.edu) or David D. Ho (dh2994@cumc.columbia.edu), Columbia University Vagelos College of Physicians and Surgeons, 701 W. 168th Street, New York, NY 10032, USA.

Abstract

SARS-CoV-2 Omicron subvariants BA.2.12.1 and BA.4/5 have surged dramatically to become dominant in the United States and South Africa, respectively[1,2]. These novel subvariants carrying additional mutations in their spike proteins raise concerns that they may further evade neutralizing antibodies, thereby further compromising the efficacy of COVID-19 vaccines and therapeutic monoclonals. We now report findings from a systematic antigenic analysis of these surging Omicron subvariants. BA.2.12.1 is only modestly (1.8-fold) more resistant to sera from vaccinated and boosted individuals than BA.2. However, BA.4/5 is substantially (4.2-fold) more resistant and thus more likely to lead to vaccine breakthrough infections. Mutation at spike residue L452 found in both BA.2.12.1 and BA.4/5 facilitates escape from some antibodies directed to the so-called class 2 and 3 regions of the receptor-binding domain[3]. The F486V mutation found in BA.4/5 facilitates escape from certain class 1 and 2 antibodies but compromises the spike affinity for the viral receptor. The R493Q reversion mutation, however, restores receptor affinity and consequently the fitness of BA.4/5. Among therapeutic antibodies authorized for clinical use, only bebtelovimab retains full potency against both BA.2.12.1 and BA.4/5. The Omicron lineage of SARS-CoV-2 continues to evolve, successively yielding subvariants that are not only more transmissible but also more evasive to antibodies.

Main text

Severe acute respiratory syndrome coronavirus 2 (SARS-CoV-2) Omicron or B.1.1.529 variant continues to dominate the coronavirus disease 2019 (COVID-19) pandemic. Globally, the BA.2 subvariant has rapidly replaced previous subvariants BA.1 and BA.1.1 (Fig. 1a). The recent detection and dramatic expansion of three new Omicron subvariants have raised concerns. BA.2.12.1 emerged in the United States in early February and expanded substantially (Fig. 1a), now accounting for over 55% of all new SARS-CoV-2 infections in the country[2]. BA.4 and BA.5 emerged in South Africa in January and rapidly became dominant there with a combined frequency of over 88%[4]. These new Omicron subvariants have been detected worldwide, with a combined frequency of over 50% in recent weeks. However, their growth trajectories in the U.S. and South Africa indicate a significant transmission advantage that will likely result in further expansion, as is being observed in countries such as the United Kingdom (Fig. 1a). Phylogenetically, these new subvariants evolved independently from BA.2 (Fig. 1b). The spike protein of BA.2.12.1 contains L452Q and S704L alterations in addition to the known mutations in BA.2, whereas the spike proteins of BA.4 and BA.5 are identical, each with four additional alterations: Del69-70, L452R, F486V, and R493Q, a reversion mutation (Fig. 1c). The location of several of these mutations within RBD of the spike protein raises the specter that BA.2.12.1 and BA.4/5 may have evolved to further escape from neutralizing antibodies.

Neutralization by monoclonal antibodies

To understand antigenic differences of BA.2.12.1 and BA.4/5 from previous Omicron subvariants (BA.1, BA.1.1, and BA.2) and the wild-type SARS-CoV-2 (D614G), we produced each pseudovirus and then assessed the sensitivity of each pseudovirus to neutralization by a panel of 21 monoclonal antibodies (mAbs) directed to known neutralizing epitopes on the viral spike. Among these, 19 target the four epitope classes in the receptor binding domain (RBD)[3], including REGN10987 (imdevimab)[5], REGN10933 (casirivimab)[5], COV2-2196 (tixagevimab)[6], COV2-2130 (cilgavimab)[6], LY-CoV555 (bamlanivimab)[7], CB6 (etesevimab)[8], Brii-196 (amubarvimab)[9], Brii-198 (romlusevimab)[9], S309 (sotrovimab)[10], LY-CoV1404 (bebtelovimab)[11], ADG-2[12], DH1047[13], S2X259[14], CAB-A17[15] and ZCB11[16], as well as 1-20, 2-15, 2-7[17] and 10-40[18] from our group. Two other mAbs, 4-18 and 5-7[17], target the N-terminal domain (NTD). Our findings are shown in Fig. 2a, as well as in Extended Data Fig. 1 and Table 1. Overall, 18 and 19 mAbs lost

neutralizing activity completely or partially against BA.2.12.1 and BA.4/5, respectively. Neutralization profiles were similar for BA.2 and BA.2.12.1 except for three class 3 RBD mAbs (Brii-198, REGN10987, and COV2-2130) that were either inactive or further impaired against the latter subvariant. Compared to BA.2 and BA.2.12.1, BA.4/5 showed substantially greater neutralization resistance to two class 2 RBD mAbs (ZCB11 and COV2-2196) as well as modest resistance to two class 3 RBD mAbs (REGN10987 and COV2-2130). Collectively, these differences suggest that mutations in BA.2.12.1 confer greater evasion from antibodies to class 3 region of RBD, whereas mutations in BA.4/5 confer greater evasion from antibodies to class 2 and class 3 regions. Only four RBD mAbs (CAB-A17, COV2-2130, 2-7, and LY-COV1404) retained good in vitro potency against both BA.2.12.1 and BA.4/5 with IC_{50} below 0.1 μg/mL. Importantly, among these four mAbs, COV2-2130 (cilgavimab) is one component of a combination known as Evusheld that is authorized for prevention of COVID-19, while only LY-COV1404 or bebtelovimab is authorized for therapeutic use in the clinic. For antibody combinations previously authorized or approved for clinical use, all showed a substantial loss of activity in vitro against BA.2.12.1 and BA.4/5. As for a mAb directed to the antigenic supersite of N-terminal domain (NTD)[19], 4-18 lost neutralizing activity against all Omicron subvariants. A mAb to the NTD alternate site, 5-7[20], was also inactive against BA.2.12.1 and BA.4/5 but retained modest activity against BA.1 and BA.1.1 (Fig. 2a).

A subset of the pseudovirus neutralization data was confirmed for four monoclonal antibodies (COV2-2196, ZCB11, REGN10987, and LY-CoV1404) in neutralization experiments using authentic viruses BA.2 and BA.4 (Extended Data Fig. 1b and Table 1b). Similar neutralization patterns were observed in the two assays, although the precise 50% neutralizing titers were different.

To identify the mutations in BA.2.12.1 and BA.4/5 that confer antibody resistance, we assessed the neutralization sensitivity of pseudoviruses carrying each of the point mutations in the background of D614G or BA.2 to the aforementioned panel of mAbs and combinations. Detailed findings are presented in Extended Data Figs. 2, 3, and Table 2, and most salient results are highlighted in Fig. 2b and discussed here. Substitutions (M, R, and Q) at residue L452, previously found in the Delta and Lambda variants[21,22], conferred resistance largely to classes 2 and 3 RBD

mAbs, with L452R being the more detrimental mutation. F486V broadly impaired the neutralizing activity of several class 1 and 2 RBD mAbs. Notably, this mutation decreased the potency of ZCB11 by >2000-fold. In contrast, the reversion mutation R493Q sensitized BA.2 to neutralization by several class 1 and 2 RBD mAbs. This finding is consistent with our previous study[23] showing that Q493R found in the earlier Omicron subvariants mediated resistance to the same set of mAbs. L452, F486, and Q493, situated at the top of RBD, are among the residues most commonly targeted by SARS-CoV-2 neutralizing mAbs whose epitopes have been defined (Fig. 2c). In silico structural analysis showed that both L452R and L452Q caused steric hindrance to the binding by class 2 RBD mAbs. One such example is shown for LY-CoV555 (Fig. 2d), demonstrating the greater clash because of the arginine substitution and explaining why this particular mutation led to a larger loss of virus-neutralizing activity (Fig. 2b). Structural modeling of the F486V again revealed steric hindrance to binding by class 2 RBD mAbs such as REGN10933, LY-CoV555, and 2-15 caused by the valine substitution (Fig. 2e).

Receptor affinity

Epidemiological data clearly indicate that both BA.2.12.1 and BA.4/5 are very transmissible (Fig. 1a); however, the additional mutations at the top of RBD (Fig. 2c) of these subvariants raises the possibility of a significant loss of affinity for the viral receptor, human angiotensin-converting enzyme 2 (hACE2). We therefore measured the binding affinity of purified spike proteins of D614G and major Omicron subvariants to dimeric hACE2 using surface plasmon resonance (SPR). The spike proteins of the Omicron subvariants exhibited similar binding affinities to hACE2, with K_D values ranging from 1.66 nM for BA.4/5 to 2.36 nM for BA.2.12.1 to 2.79 nM for BA.1.1 (Fig. 3a). Impressively, despite having $\geq$17 mutations in the RBD including some that mediate antibody escape, BA.2.12.1 and BA.4/5 also evolved concurrently to gain a slightly higher affinity for the receptor than an ancestral SARS-CoV-2, D614G (K_D 5.20 nM).

To support the findings by SPR and to probe the role of point mutations in hACE2 binding, we tested BA.2, BA.2.12.1, and BA.4/5 pseudoviruses, as well as pseudoviruses containing key mutations, to neutralization by dimeric hACE2 in vitro. The 50% inhibitory concentration (IC_{50}) values were lower for BA.4/5 and BA.2.12.1 than that of BA.2 (Fig. 3b), again indicating that these two emerging Omicron subvariants have not lost receptor affinity. Our results also showed

that the F486V mutation compromised receptor affinity, as previously reported[24], while the R493Q reversion mutation improved receptor affinity. To structurally interpret these results, we modeled F486V and R493Q mutations based on the crystal structure of BA.1-RBD-hACE2 complex[25] overlaid with ligand-free BA.2 RBD (PDB: 7U0N and 7UB0). This analysis found that both R493 and F486 are conformationally similar between BA.1 and BA.2, and F486V led to a loss of interaction with a hydrophobic pocket in hACE2 (Fig. 3c). On the other hand, the R493Q reversion mutation restored a hydrogen bond with H34 and avoided the charge repulsion by K31, seemingly having the opposite effect of F486V. Interestingly, the mutation frequency at F486 had been exceedingly low (<10E-5) until the emergence of BA.4/5 (Extended Data Table 3), probably because of a compromised receptor affinity. Taken together, our findings in Figs. 2 and 3 suggest that F486V allowed BA.4 and BA.5 to extend antibody evasion while R493Q compensated to regain fitness in receptor binding.

Neutralization by polyclonal sera

We next assessed the extent of BA.2.12.1 and BA.4/5 resistance to neutralization by sera from four different clinical cohorts. Sera from persons immunized with only two doses of COVID-19 mRNA vaccines were not examined because most of them could not neutralize earlier Omicron subvariants[23,26]. Instead, we measured serum neutralizing activity for persons who received three shots of mRNA vaccines (boosted), individuals who received mRNA vaccines before or after non-Omicron infection, and patients with either BA.1 or BA.2 breakthrough infection after vaccination. Their clinical information is described in Extended Data Table 4, and the serum neutralization profiles are presented in Extended Data Fig. 4 and the 50% inhibitory dose (ID_{50}) titers are summarized in Fig. 4a. For the "boosted" cohort, neutralization titers were noticeably lower (4.6-fold to 6.2-fold) for BA.1, BA.1.1, and BA.2 compared to D614G (Fig. 4b), as previously reported[23,26]. Titers for BA.2.12.1 and BA.4/5 were even lower, by 8.1-fold and 19.2-fold, respectively, relative to D614G, and by 1.8-fold and 4.2-fold, respectively, relative to BA.2. A similar trend was observed for serum neutralization for the other cohorts, with the lowest titers against BA.4/5, followed next by titers against BA.2.12.1. Relative to BA.2, BA.2.12.1 and BA.4/5 showed 1.2-fold to 1.4-fold and 1.6-fold to 4.3-fold, respectively, greater resistance to neutralization by sera from these individuals who had both mRNA vaccination and SARS-CoV-2 infection. In addition, sera from vaccinated and boosted individuals were assayed for

neutralization of authentic viruses (Extended Data Figs. 4e and 4f). Neutralization titers for BA.4 were 2.7-fold lower on average compared to titers for BA.2, in line with the pseudovirus results.

We also conducted serum neutralization assays on pseudoviruses containing point mutations found in BA.2.12.1 or BA.4/5 in the background of BA.2. Del69-70, L452M/R/Q, and F486V each modestly (1.1-fold to 2.4-fold) decreased the neutralizing activity of sera from all cohorts, while the R493Q reversion mutation modestly (~1.5-fold) enhanced the neutralization (Fig. 4c and Extended Data Fig. 5). S704L, a mutation close to the S1/S2 cleavage site, did not appreciably alter the serum neutralization titers against BA.2. For "boosted" serum samples, the impact of each point mutant on neutralization resistance was quantified and summarized in Fig. 4b.

Using these serum neutralization results, we then constructed a graphic display to map antigenic distances among D614G, various Omicron subvariants, and individual point mutants using only results from the "boosted" serum samples to avoid confounding effects from differences in clinical histories in the other cohorts. Utilizing methods well established in influenza research[27], all virus and serum positions on the antigenic map were optimized so that the distances between them correspond to the fold drop in neutralizing ID_{50} titer relative to the maximum titer for each serum. Each unit of distance in any direction on the antigenic map corresponds to a two-fold change in ID_{50} titer. The resultant antigenic cartography (Fig. 4d) shows that BA.1, BA.1.1, and BA.2 are approximately equidistant from the "boosted" sera, with each about 2-3 antigenic units away. BA.2.12.1 is further away from BA.2 by about 1 antigenic unit. Most strikingly, BA.4/5 is 4.3 antigenic units further from "boosted" sera than D614G, and 2 antigenic units further than BA.2. Each of the point mutants Del69-70, L452M/Q/R, and F486V adds antigenic distance from these sera compared to BA.2 and D614G, whereas R493Q has the opposite effect. Overall, this map makes clear that BA.4/5 is substantially more neutralization resistant to sera obtained from boosted individuals, with several mutations contributing to the antibody evasion.

Discussion

We have systematically evaluated the antigenic properties of SARS-CoV-2 Omicron subvariants BA.2.12.1 and BA.4/5, which are rapidly expanding globally (Fig. 1a). It is apparent that BA.2.12.1 is only modestly (1.8-fold) more resistant to sera from vaccinated and boosted

individuals than the BA.2 subvariant that currently dominates the global pandemic (Figs. 4b). On the other hand, BA.4/5 is substantially (4.2-fold) more resistant, a finding consistent with results recently posted by other groups[1,28]. This antigenic distance is similar to that between the Delta variant and the ancestral virus[29] and thus is likely to lead to more breakthrough infections in the coming months. A key question now is whether BA.4/5 would out-compete BA.2.12.1, which poses less of an antigenic threat. This competition is now playing out in the United Kingdom. These new Omicron subvariants were first detected there almost simultaneously in late March of 2022. However, BA.2.12.1 now accounts for 13% of new infections in the U.K., whereas the frequency is over 50% for BA.4/5 (Fig. 1a), suggesting a transmission advantage for the latter.

Epidemiologically, since both of these two Omicron subvariants have a clear advantage in transmission, it is therefore not surprising that their abilities to bind the hACE2 receptor remain robust (Fig. 3a) despite numerous mutations in the spike protein. In fact, BA.4/5 may have slightly higher affinity for the receptor, consistent with suggestions that it might be more fit[30]. However, assessment of transmissibility would be more revealing by conducting studies on BA.2.12.1 and BA.4/5 in animal models[31].

Our studies on the specific mutations found in BA.2.12.1 and BA.4/5 show that Del69-70, L452M/R/Q, and F486V could individually contribute to antibody resistance, whereas R493Q confers antibody sensitivity (Fig. 4b). Moreover, the data generated using SARS-CoV-2-neutralizing mAbs suggest that a mutation at L452 allows escape from class 2 and class 3 RBD antibodies and that the F486V mutation mediates escape from class 1 and class 2 RBD antibodies (Fig. 2b). It is not clear how Del69-70, a mutation that might increase infectivity[32] and previously seen in the Alpha variant[33], contributes to antibody resistance except for the possible evasion from certain neutralizing antibodies directed to the NTD. As for the use of clinically authorized mAbs to treat or block infection by BA.2.12.1 or BA.4/5, only bebtelovimab (LY-COV1404)[11] retains exquisite potency while the combination of tixagevimab and cilgavimab (COV2-2196 and COV2-2130)[6] shows a modest loss of activity (Fig. 2a).

As the Omicron lineage has evolved over the past few months (Fig. 1b), each successive subvariant has seemingly become better and better at human transmission (Fig. 1a) as well as in antibody evasion[23,34]. It is only natural that scientific attention remains intently focused on each new subvariant of Omicron. However, we must be mindful that each of the globally dominant variants of SARS-CoV-2 (Alpha, Delta, and Omicron) emerged stochastically and unexpectedly. Vigilance in our collective surveillance effort must be sustained.

References

1 Khan, K. *et al.* Omicron sub-lineages BA.4/BA.5 escape BA.1 infection elicited neutralizing immunity. *medRxiv*, doi:10.1101/2022.04.29.22274477 (2022).

2 Centers for Disease Control and Prevention. *COVID Data Tracker*, <https://covid.cdc.gov/covid-data-tracker/#variant-proportions> (2022).

3 Barnes, C. O. *et al.* SARS-CoV-2 neutralizing antibody structures inform therapeutic strategies. *Nature* **588**, 682-687, doi:10.1038/s41586-020-2852-1 (2020).

4 Shu, Y. & McCauley, J. GISAID: Global initiative on sharing all influenza data - from vision to reality. *Euro Surveill* **22**, doi:10.2807/1560-7917.ES.2017.22.13.30494 (2017).

5 Hansen, J. *et al.* Studies in humanized mice and convalescent humans yield a SARS-CoV-2 antibody cocktail. *Science* **369**, 1010-1014, doi:10.1126/science.abd0827 (2020).

6 Zost, S. J. *et al.* Potently neutralizing and protective human antibodies against SARS-CoV-2. *Nature* **584**, 443-449, doi:10.1038/s41586-020-2548-6 (2020).

7 Jones, B. E. *et al.* The neutralizing antibody, LY-CoV555, protects against SARS-CoV-2 infection in nonhuman primates. *Sci Transl Med* **13**, doi:10.1126/scitranslmed.abf1906 (2021).

8 Shi, R. *et al.* A human neutralizing antibody targets the receptor-binding site of SARS-CoV-2. *Nature* **584**, 120-124, doi:10.1038/s41586-020-2381-y (2020).

9 Ju, B. *et al.* Human neutralizing antibodies elicited by SARS-CoV-2 infection. *Nature* **584**, 115-119, doi:10.1038/s41586-020-2380-z (2020).

10 Pinto, D. *et al.* Cross-neutralization of SARS-CoV-2 by a human monoclonal SARS-CoV antibody. *Nature* **583**, 290-295, doi:10.1038/s41586-020-2349-y (2020).

11 Westendorf, K. *et al.* LY-CoV1404 (bebtelovimab) potently neutralizes SARS-CoV-2 variants. *Cell Rep* **39**, 110812, doi:10.1016/j.celrep.2022.110812 (2022).

12 Rappazzo, C. G. *et al.* Broad and potent activity against SARS-like viruses by an engineered human monoclonal antibody. *Science* **371**, 823-829, doi:10.1126/science.abf4830 (2021).

13 Li, D. *et al.* In vitro and in vivo functions of SARS-CoV-2 infection-enhancing and neutralizing antibodies. *Cell* **184**, 4203-4219 e4232, doi:10.1016/j.cell.2021.06.021 (2021).

14 Tortorici, M. A. *et al.* Broad sarbecovirus neutralization by a human monoclonal antibody. *Nature* **597**, 103-108, doi:10.1038/s41586-021-03817-4 (2021).

15 Sheward, D. J. *et al.* Structural basis of Omicron neutralization by affinity-matured public antibodies. *bioRxiv*, doi:10.1101/2022.01.03.474825 (2022).

16 Zhou, B. *et al.* An elite broadly neutralizing antibody protects SARS-CoV-2 Omicron variant challenge. *bioRxiv*, doi:10.1101/2022.01.05.475037 (2022).

17 Liu, L. *et al.* Potent neutralizing antibodies against multiple epitopes on SARS-CoV-2 spike. *Nature* **584**, 450-456, doi:10.1038/s41586-020-2571-7 (2020).

18 Liu, L. *et al.* An antibody class with a common CDRH3 motif broadly neutralizes sarbecoviruses. *Sci Transl Med*, eabn6859, doi:10.1126/scitranslmed.abn6859 (2022).

19 Cerutti, G. *et al.* Potent SARS-CoV-2 neutralizing antibodies directed against spike N-terminal domain target a single supersite. *Cell Host Microbe* **29**, 819-833 e817, doi:10.1016/j.chom.2021.03.005 (2021).

20 Cerutti, G. *et al.* Neutralizing antibody 5-7 defines a distinct site of vulnerability in SARS-CoV-2 spike N-terminal domain. *Cell Rep* **37**, 109928, doi:10.1016/j.celrep.2021.109928 (2021).

21 Planas, D. *et al.* Reduced sensitivity of SARS-CoV-2 variant Delta to antibody neutralization. *Nature* **596**, 276-280, doi:10.1038/s41586-021-03777-9 (2021).

22 Kimura, I. *et al.* The SARS-CoV-2 Lambda variant exhibits enhanced infectivity and immune resistance. *Cell Rep* **38**, 110218, doi:10.1016/j.celrep.2021.110218 (2022).

23 Liu, L. *et al.* Striking antibody evasion manifested by the Omicron variant of SARS-CoV-2. *Nature* **602**, 676-681, doi:10.1038/s41586-021-04388-0 (2022).

24 Starr, T. N. *et al.* Shifting mutational constraints in the SARS-CoV-2 receptor-binding domain during viral evolution. *bioRxiv*, doi:10.1101/2022.02.24.481899 (2022).

25 Geng, Q. *et al.* Structural Basis for Human Receptor Recognition by SARS-CoV-2 Omicron Variant BA.1. *J Virol* **96**, e0024922, doi:10.1128/jvi.00249-22 (2022).
26 Iketani, S. *et al.* Antibody evasion properties of SARS-CoV-2 Omicron sublineages. *Nature* **604**, 553-556, doi:10.1038/s41586-022-04594-4 (2022).
27 Smith, D. J. *et al.* Mapping the antigenic and genetic evolution of influenza virus. *Science* **305**, 371-376, doi:10.1126/science.1097211 (2004).
28 Tuekprakhon, A. *et al.* Antibody escape of SARS-CoV-2 Omicron BA.4 and BA.5 from vaccine and BA.1 serum. *Cell*, doi:https://doi.org/10.1016/j.cell.2022.06.005 (2022).
29 Rössler, A. *et al.* BA.2 omicron differs immunologically from both BA.1 omicron and pre-omicron variants. *medRxiv*, doi:10.1101/2022.05.10.22274906 (2022).
30 Cao, Y. *et al.* BA.2.12.1, BA.4 and BA.5 escape antibodies elicited by Omicron infection. *Nature*, doi:10.1038/s41586-022-04980-y (2022).
31 Munoz-Fontela, C. *et al.* Animal models for COVID-19. *Nature* **586**, 509-515, doi:10.1038/s41586-020-2787-6 (2020).
32 Chen, Y. *et al.* Emerging SARS-CoV-2 variants: Why, how, and what's next? *Cell Insight* **1**, 100029, doi:https://doi.org/10.1016/j.cellin.2022.100029 (2022).
33 Wang, R. *et al.* Analysis of SARS-CoV-2 variant mutations reveals neutralization escape mechanisms and the ability to use ACE2 receptors from additional species. *Immunity* **54**, 1611-1621 e1615, doi:10.1016/j.immuni.2021.06.003 (2021).
34 Yu, J. *et al.* Neutralization of the SARS-CoV-2 Omicron BA.1 and BA.2 Variants. *N Engl J Med* **386**, 1579-1580, doi:10.1056/NEJMc2201849 (2022).
35 Wrapp, D. *et al.* Cryo-EM structure of the 2019-nCoV spike in the prefusion conformation. *Science* **367**, 1260-1263, doi:10.1126/science.abb2507 (2020).
36 Krissinel, E. & Henrick, K. Inference of macromolecular assemblies from crystalline state. *J Mol Biol* **372**, 774-797, doi:10.1016/j.jmb.2007.05.022 (2007).
37 Cerutti, G. *et al.* Structural basis for accommodation of emerging B.1.351 and B.1.1.7 variants by two potent SARS-CoV-2 neutralizing antibodies. *Structure* **29**, 655-663 e654, doi:10.1016/j.str.2021.05.014 (2021).

Figure legends

Fig. 1 | Prevalence of SARS-CoV-2 Omicron subvariants. a, Frequencies of BA.1, BA.1.1, BA.2, BA.2.12.1, and BA.4/5 deposited in GISAID. The value in the upper right corner of each box denotes the cumulative number of sequences for all circulating viruses in the denoted time period. **b**, Unrooted phylogenetic tree of Omicron and its subvariants along with other major SARS-CoV-2 variants. The scale bar indicates the genetic distance. **c**, Key spike mutations found in BA.2, BA.2.12.1, BA.4, and BA.5. Del, deletion.

Fig. 2 | Resistance of Omicron subvariants to neutralization by monoclonal antibodies. a, Neutralization of D614G and Omicron subvariants by RBD- and NTD-directed mAbs. Values above the limit of detection of 10 μg/mL (dotted line) are arbitrarily plotted to allow for visualization of each sample. **b**, Fold change in IC_{50} values of point mutants relative to D614G or BA.2, with resistance colored red and sensitization colored green. **c**, Location of F486V, L452R/Q, and R493Q on D614G RBD, with the color indicating the per residue frequency recognized by SARS-CoV-2 neutralizing antibodies. Modeling of L452R/Q (**d**) and F486V (**e**) affect class 2 mAb neutralization. The clashes are shown in red plates; the hydrogen bonds are shown in dark dashed lines. The results shown in **a** and **b** are representative of those obtained in two independent experiments.

Fig. 3 | Affinity of the spike proteins of SARS-CoV-2 Omicron subvariants to hACE2. a, Binding affinities of Omicron subvariant S2P spike proteins to hACE2 as measured by SPR. **b**, Sensitivity of pseudotyped Omicron subvariants and the individual mutations in the background of BA.2 to hACE2 inhibition. The hACE2 concentrations resulting in 50% inhibition of infectivity (IC_{50}) are presented. Data are shown as mean ± standard error of mean (SEM) for three technical replicates. **c**, In silico analysis for how R493Q and F486V affect hACE2 binding. The hACE2 surface is shown with charge potential, with red and blue representing negative and positive charges, respectively. Omicron BA.1 RBD in complex with hACE2 was downloaded from PDB 7U0N, and the ligand-free BA.2 RBD was downloaded from PDB 7UB0. The results shown in **a** and **b** are representative of those obtained in two independent experiments.

Fig. 4 | BA.2.12.1 and BA.4/5 exhibit greater serum neutralization resistance profiles relative to BA.2. a, Neutralization of pseudotyped D614G and Omicron subvariants by sera from 4 different clinical cohorts. **b**, Fold change in geometric mean ID_{50} titers of boosted vaccinee sera

relative to D614G and BA.2, with resistance colored red and sensitization colored green. **c**, Serum neutralization of BA.2 pseudoviruses containing single mutations found within BA.2.12.1 and BA.4/5. **d**, Antigenic map based on the neutralization data of boosted vaccinee sera. SARS-CoV-2 variants are shown as colored circles and sera are shown as grey squares. The x-, y-, and z-axis represent antigenic units (AU) with one grid corresponding to a two-fold serum dilution of the neutralization titer. An interactive map is available online (https://figshare.com/articles/media/OmicronAntigenicMap/19854046). The map orientation within the x-, y-, and z-axis is free to rotate. For all the panels in **a** and **c**, values above the symbols denote the geometric mean ID_{50} values and values on the lower left show the sample size (n) for each group. *P* values were determined by using two-tailed Wilcoxon matched-pairs signed-rank tests. The results shown are representative of those obtained in two independent experiments.

Methods

Data reporting

No statistical methods were used to predetermine sample size. The experiments were not randomized and the investigators were not blinded to allocation during experiments and outcome assessment.

Serum samples

Sera from individuals who received three doses of the mRNA-1273 or BNT162b2 vaccine were collected at Columbia University Irving Medical Center. Sera from individuals who were infected by non-Omicron variants of SARS-CoV-2 in addition to vaccination were collected from January 2021 to September 2021 at Columbia University Irving Medical Center or at the Hackensack Meridian Center for Discovery and Innovation (CDI). Sera from individuals who were infected by Omicron (BA.1 or BA.2) following vaccinations were collected from December 2021 to May 2022 at Columbia University Irving Medical Center. All samples were confirmed for prior SARS-CoV-2 infection status by anti-nucleoprotein (NP) ELISA. All collections were conducted under protocols reviewed and approved by the Institutional Review Board of Columbia University or the Hackensack Meridian Center for Discovery and Innovation. All participants provided written informed consent. Clinical information on the different cohorts of study subjects is provided in Extended Data Table 4.

Monoclonal antibodies

Antibodies were expressed as previously described[17]. Heavy chain variable (VH) and light chain variable (VL) genes for each antibody were synthesized (GenScript), then transfected into Expi293 cells (Thermo Fisher Scientific), and purified from the supernatant by affinity purification using rProtein A Sepharose (GE). REGN10987, REGN10933, COV2-2196, and COV2-2130 were provided by Regeneron Pharmaceuticals; Brii-196 and Brii-198 were provided by Brii Biosciences; CB6 was provided by B. Zhang and P. Kwong (NIH); and ZCB11 was provided by Z. Chen (HKU).

Cell lines

Expi293 cells were obtained from Thermo Fisher Scientific (A14527); Vero-E6 cells were obtained from the ATCC (CRL-1586); HEK293T cells were obtained from the ATCC (CRL-3216). Cells were purchased from authenticated vendors and morphology was confirmed visually before use. All cell lines tested mycoplasma negative.

Variant SARS-CoV-2 spike plasmid construction

BA.1, BA.1.1, and BA.2 spike-expressing plasmids were generated as previously described[23,26]. Plasmids encoding the BA.2.12.1 and BA.4/5 spikes, as well as the individual and double mutations found in BA.2.12.1 and BA.4/5, were generated using the QuikChange II XL site-directed mutagenesis kit according to the manufacturer's instructions (Agilent). To make the constructs for expression of stabilized soluble S2P spike trimer proteins, 2P substitutions (K986P and V987P) and a "GSAS" substitution of the furin cleavage site (682-685aa in WA1) were introduced into the spike-expressing plasmids[35], and then the ectodomain (1-1208aa in WA1) of the spike was fused with a C-terminal 8x His-tag and cloned into the **paH** vector. All constructs were confirmed by Sanger sequencing.

Expression and purification of SARS-CoV-2 S2P spike proteins

SARS-CoV-2 S2P spike trimer proteins of the D614G and Omicron subvariants were generated by transfecting Expi293 cells with the S2P spike trimer-expressing constructs using 1 mg mL^{-1} polyethylenimine (PEI) and then purifying from the supernatants five days post-transfection using Ni-NTA resin (Invitrogen) according to the manufacturer's instructions[17].

Surface plasmon resonance

Surface plasmon resonance (SPR) binding assays for hACE2 binding to SARS-CoV-2 S2P spike were performed using a Biacore T200 biosensor equipped with a Series S CM5 chip (Cytiva), in a running buffer of 10 mM HEPES pH 7.4, 150 mM NaCl, 3 mM EDTA, 0.05% P-20 (Cytiva) at 25 °C. Spike proteins were captured through their C-terminal His-tag over an anti-His antibody surface. These surfaces were generated using the His-capture kit (Cytiva) according to the manufacturer's instructions, resulting in approximately 10,000 RU of anti-His antibody over each surface. An anti-His antibody surface without antigen was used as a reference flow cell to remove bulk shift changes from the binding signal.

Binding of human ACE2-Fc protein (Sino Biological) was tested using a three-fold dilution series with concentrations ranging from 2.46 nM to 200 nM. The association and dissociation rates were each monitored for 60 s and 300 s respectively, at 30 µL/min. The bound spike/ACE2 complex was regenerated from the anti-His antibody surface using 10 mM glycine pH 1.5. Blank buffer cycles were performed by injecting running buffer instead of human ACE2-Fc to remove systematic noise from the binding signal. The resulting data was processed and fit to a 1:1 binding model using Biacore Evaluation Software.

Pseudovirus production

Pseudoviruses were produced in the vesicular stomatitis virus (VSV) background, in which the native glycoprotein was replaced by that of SARS-CoV-2 and its variants, as previously described[17]. In brief, HEK293T cells were transfected with a spike expression construct with 1 mg mL^{-1} polyethylenimine (PEI) and cultured overnight at 37 °C under 5% CO_2, and then infected with VSV-G pseudotyped ΔG-luciferase (G*ΔG-luciferase, Kerafast) one day post-transfection. After 2 h of infection, cells were washed three times, changed to fresh medium, and then cultured for approximately another 24 h before the supernatants were collected, clarified by centrifugation, and aliquoted and stored at -80 °C for further use.

Pseudovirus neutralization assay

All viruses were first titrated to normalize the viral input between assays. Heat-inactivated sera or antibodies were first serially diluted (five-fold) in medium in 96-well plates in triplicate, starting at 1:100 dilution for sera and 10 µg mL^{-1} for antibodies. Pseudoviruses were then added and the virus–sample mixture was incubated at 37 °C for 1 h. Vero-E6 cells were then added at a density of 3×10^4 cells per well and the plates were incubated at 37 °C for approximately 10 h. Luciferase activity was quantified using the Luciferase Assay System (Promega) according to the manufacturer's instructions using SoftMax Pro v.7.0.2 (Molecular Devices). Neutralization curves and IC_{50} values were derived by fitting a nonlinear five-parameter dose-response curve to the data in GraphPad Prism v.9.2.

Authentic virus neutralization assay

The SARS-CoV-2 viruses hCoV-19/USA/CO-CDPHE-2102544747/2021 (BA.2) and hCoV-19/USA/MD-HP30386/2022 (BA.4) were obtained from BEI Resources (NIAID, NIH) and propagated by passaging in Vero-E6 cells. Virus infectious titers were determined by an end-point dilution and cytopathogenic effect assay on Vero-E6 cells as previously described[17].

An end-point dilution microplate neutralization assay was performed to measure the neutralization activity of sera from vaccinated and boosted individuals as well as of purified monoclonal antibodies. In brief, serum samples were subjected to successive five-fold dilutions starting from 1:100. Monoclonal antibodies were serially diluted (five-fold) starting at 5 μg/ml. Triplicates of each dilution were incubated with SARS-CoV-2 at a multiplicity of infection of 0.1 in EMEM with 7.5% inactivated fetal calf serum for 1 h at 37 °C. After incubation, the virus–antibody mixture was transferred onto a monolayer of Vero-E6 cells grown overnight. The cells were incubated with the mixture for around 70 h. Cytopathogenic effects of viral infection were visually scored for each well in a blinded manner by two independent observers. The results were then converted into the percentage of neutralization at a given sample dilution or monoclonal antibody concentration, and the data (mean ± SEM) were plotted using a five-parameter dose-response curve in GraphPad Prism v.9.2.

Antibody targeting frequency and mutagenesis analysis for RBD

The SARS-CoV-2 spike structure (6ZGE) used for displaying epitope footprints was downloaded from the Protein Data Bank (PDB). Epitope residues were identified using PISA[36] with default parameters, and the RBD residues with non-zero buried accessible surface area were considered epitope residues. For each residue within the RBD, the frequency of antibody recognition was calculated as the number of contact antibodies[37]. The structures of antibody-spike complexes for modeling were also obtained from PDB (7L5B (2-15), 6XDG (REGN10933), and 7KMG (LY-CoV555)). Omicron BA.1 RB D in complex with hACE2 was downloaded from PDB 7U0N, and the ligand-free BA.2 RBD was downloaded from PDB 7UB0. PyMOL v.2.3.2 was used to perform mutagenesis and to generate structural plots (Schrödinger, LLC).

Antigenic cartography

449 The antigenic distances between SARS-CoV-2 variants were approximated by incorporating the
450 neutralization potency of each serum sample into a previously described antigenic cartography
451 approach[27]. The map was generated by the Racmacs package (https://acorg.github.io/Racmacs/,
452 version 1.1.4) in R with the optimization steps set to 2000, and with the minimum column basis
453 parameter set to "none".
454

Acknowledgements

This study was supported by funding from the Gates Foundation, JPB Foundation, Andrew and Peggy Cherng, Samuel Yin, Carol Ludwig, David and Roger Wu, Regeneron Pharmaceuticals, and the NIH SARS-CoV-2 Assessment of Viral Evolution (SAVE) Program. We acknowledge David S. Perlin for providing serum samples from a few COVID-19 patients. We thank all who contributed their data to GISIAD.

Author contributions

D.D.H. and L.L. conceived this project. Q.W. and L.L. conducted pseudovirus neutralization experiments and purified SARS-CoV-2 spike proteins. Y.G. and Z.S. conducted bioinformatic analyses. Q.W., L.L., and S.I. constructed the spike expression plasmids. Q.W. managed the project. J.Y. M.W., and Z.C. expressed and purified antibodies. L.L. and Z.L. performed surface plasmon resonance (SPR) assay. M.T.Y., M.E.S., J.Y.C., A.D.B. J.G.S., N.N., and K.M. provided clinical samples. H.M. aided sample collections. M.S.N. and Y.H. performed infectious SARS-CoV-2 neutralization assays. D.D.H. and L.L. directed and supervised the project. Q.W., Y.G., L.L., and D.D.H. analyzed the results and wrote the manuscript.

Competing interests

S.I, J.Y., Y.H., L.L., and D.D.H. are inventors on patent applications (WO2021236998) or provisional patent applications (63/271,627) filed by Columbia University for a number of SARS-CoV-2 neutralizing antibodies described in this manuscript. Both sets of applications are under review. D.D.H. is a co-founder of TaiMed Biologics and RenBio, consultant to WuXi Biologics and Brii Biosciences, and board director for Vicarious Surgical.

Additional information

Correspondence and requests for materials should be addressed to L.L. or D. D. H.

Data availability

All data are provided in the manuscript. Materials in this study will be made available under an appropriate Materials Transfer Agreement. Sequences for Omicron prevalence analysis were

downloaded from GISAID (https://www.gisaid.org/). The structures used for analysis in this study are available from PDB under IDs 6ZGE, 7L5B, 6XDG, 7U0N, 7UB0 and 7KMG. The interactive antigenic map based on the neutralization data of boosted vaccine sera in Figure 4d is available online (https://figshare.com/articles/media/OmicronAntigenicMap/19854046).

Extended Data Legends

Extended Data Fig. 1 | Pseudovirus (a) and authentic virus (b) neutralization curves of D614G and Omicron subvariants by monoclonal antibodies. Data are shown as mean ± SEM from three technical replicates and representative of those obtained in two independent experiments.

Extended Data Fig. 2 | Pseudovirus neutralization curves for monoclonal antibodies against individual SARS-CoV-2 mutations in the background of D614G. Data are shown as mean ± SEM from three technical replicates and representative of those obtained in two independent experiments.

Extended Data Fig. 3 | Pseudovirus neutralization curves for monoclonal antibodies against individual SARS-CoV-2 mutations in the background of BA.2. Data are shown as mean ± SEM from three technical replicates and representative of those obtained in two independent experiments.

Extended Data Fig. 4 | Neutralization curves of serum against D614G and Omicron subvariants. Neutralization by **a**, boosted vaccinee sera on pseudoviruses. **b**, non-Omicron infection & vaccination sera on pseudoviruses. **c**, BA.1 breakthrough sera on pseudoviruses. **d**, BA.2 breakthrough sera on pseudoviruses. **e**, boosted vaccinee sera on authentic viruses. **f**, Neutralization ID_{50} titers of authentic BA.2 and BA.4 by boosted vaccinee sera. Values above the symbols denote the geometric mean ID_{50} values and values on the lower left show the sample size (n). *P* values were determined by using two-tailed Wilcoxon matched-pairs signed-rank tests. Error bars in **a**, **b**, **c**, **d**, and **e** denote mean ± SEM for three technical replicates. All data are representative of those obtained in two independent experiments.

Extended Data Fig. 5 | Pseudovirus neutralization curves of serum against BA.2 and BA.2 pseudovirus carrying individual mutations. Neutralization by **a**, boosted vaccinee sera. **b**, non-Omicron infection & vaccination sera. **c**, BA.1 breakthrough sera. **d**, BA.2 breakthrough sera.

Error bars denote mean ± SEM for three technical replicates. Data are representative of those obtained in two independent experiments.

Extended Data Table. 1 | Neutralization IC_{50} values for indicated pseudoviruses (a) and authentic viruses (b) by monoclonal antibodies.

Extended Data Table. 2 | Pseudovirus neutralization IC_{50} values for monoclonal antibodies against D614G (a) and BA.2 (b) carrying individual mutations.

Extended Data Table 3 | Mutation frequencies at position F486 within different SARS-CoV-2 variants.

Extended Data Table 4 | Demographics on the clinical cohorts.

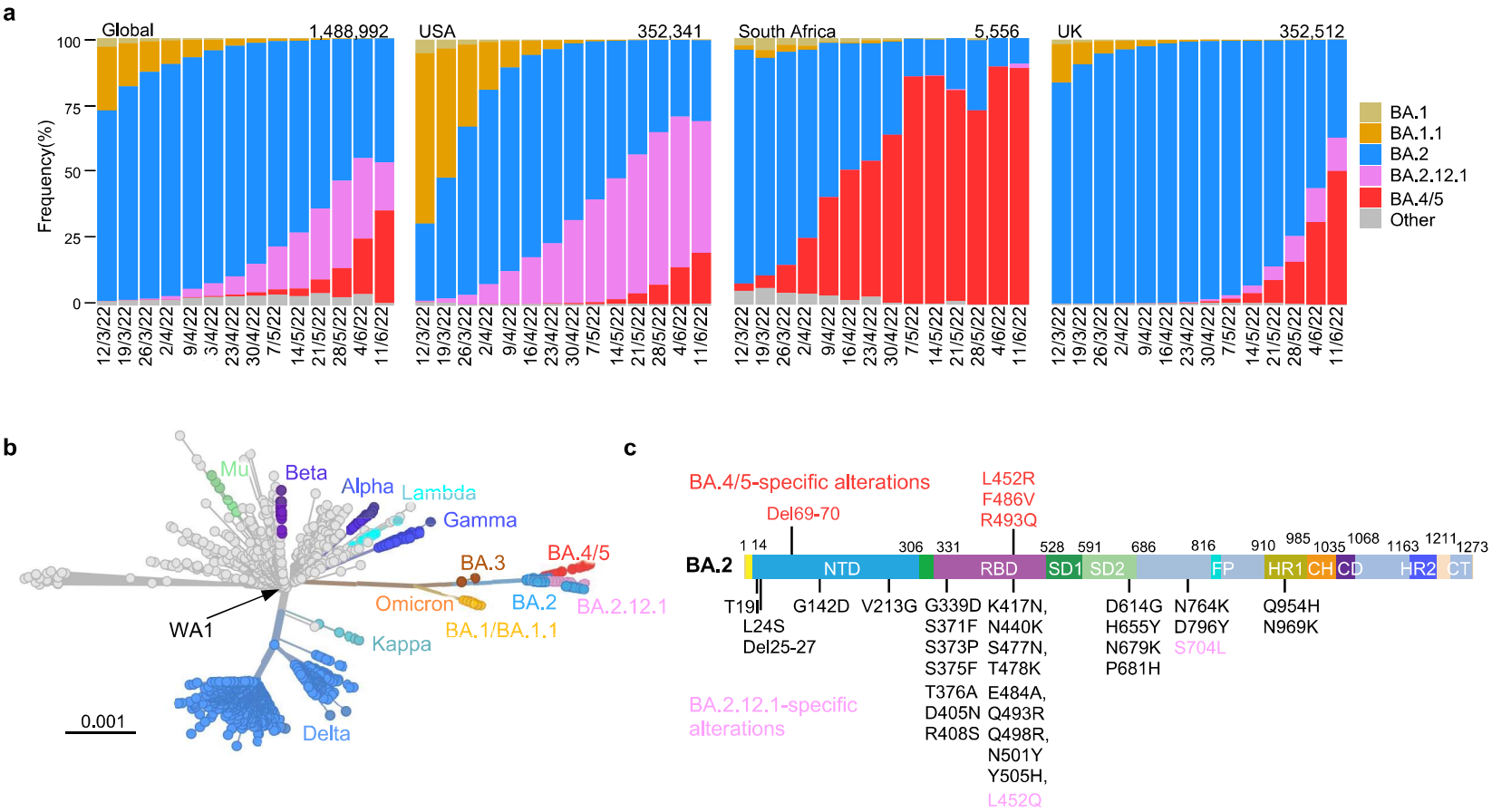
a
Global
1,488,992
USA
352,341
South Africa
5,556
UK
352,512
Frequency(%)
100
75
50
25
0
12/3/22
19/3/22
26/3/22
2/4/22
9/4/22
3/4/22
23/4/22
30/4/22
7/5/22
14/5/22
21/5/22
28/5/22
4/6/22
11/6/22
16/4/22
BA.1
BA.1.1
BA.2
BA.2.12.1
BA.4/5
Other
b
Mu
Beta
Alpha
Lambda
Gamma
BA.3
BA.4/5
Omicron
BA.2
BA.2.12.1
WA1
BA.1/BA.1.1
Kappa
0.001
Delta
c
BA.4/5-specific alterations
L452R
F486V
R493Q
Del69-70
BA.2
1 14
306
331
528
591
686
816
910
985
1035
1068
1163
1211
1273
NTD
RBD
SD1
SD2
FP
HR1
CH
CD
HR2
CT
T19I
L24S
Del25-27
G142D
V213G
G339D
S371F
S373P
S375F
T376A
D405N
R408S
K417N,
N440K
S477N,
T478K
E484A,
Q493R
Q498R,
N501Y
Y505H,
L452Q
D614G
H655Y
N679K
P681H
N764K
D796Y
S704L
Q954H
N969K
BA.2.12.1-specific
alterations

a

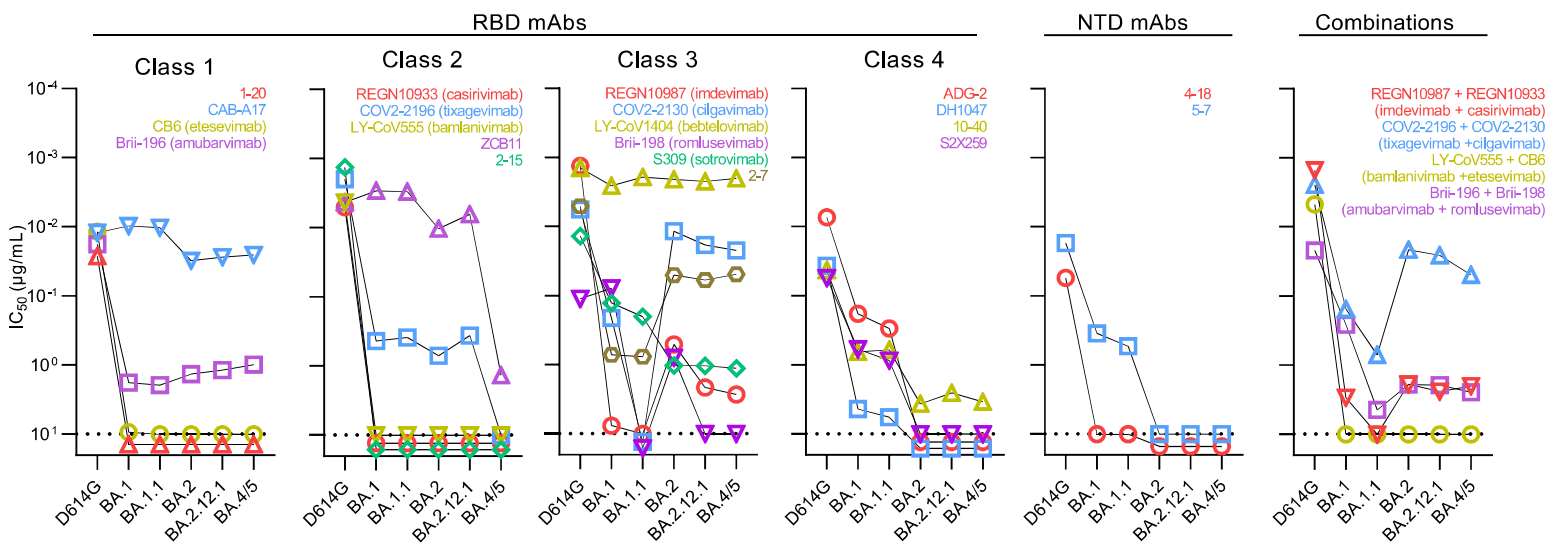

b

Fold change in IC50		RBD mAbs																			NTD mAbs		Combinations			
		Class 1				Class 2					Class 3						Class 4									
		1-20	CAB-A17	CB6	Brii-196	REGN10933	COV2-2196	LY-CoV555	ZCB11	2-15	REGN10987	COV2-2130	LY-CoV1404	Brii-198	S309	2-7	ADG-2	DH1047	10-40	S2X259	4-18	5-7	REGN10987 + REGN10933	COV2-2196 + COV2-2130	LY-CoV555 + CB6	Brii-196 + Brii-198
Compared with D614G	D614G-Del69-70	1.3	1.1	1.3	-1.3	-1.0	-1.0	2.0	-1.4	1.3	-1.3	-2.1	-1.3	-1.1	-2.0	-1.0	-1.6	-1.3	-1.7	-1.6	-1.1	-4.6	-1.7	-1.5	-1.1	-1.0
	D614G-L452M	1.5	-1.0	1.5	-1.0	<-1.9	-1.0	-1.8	-1.0	-0.9	-1.5	-1.7	-1.0	-6.9	-2.0	-1.0	-1.5	1.1	1.3	-1.0	-1.1	-1.3	-1.5	-1.1	-1.1	-1.0
	D614G-L452R	-1.2	-1.3	-1.4	-1.5	<-2.0	-1.0	-2266	-1.1	-16	-2.1	-2.6	-1.2	-27	-1.6	-1.8	-1.3	-1.0	1.4	1.8	1.1	-1.1	-1.3	-1.0	-3.9	-1.3
	D614G-L452Q	-1.3	1.1	-1.0	-1.4	<-2.1	-1.0	-5.3	-1.0	-11	-3.7	-3.8	-1.5	-18	-2.7	-2.2	-1.5	-1.5	-1.8	-1.7	-2.0	-1.6	-2.5	-1.7	-3.0	-1.9
	D614G-F486V	-1.5	-1.2	-8.1	-14	<-10000	<-272	-886	-712	-24	-1.1	-1.4	-1.3	-1.4	-1.0	-0.8	-1.4	1.1	-1.7	-2.2	1.1	-1.0	-4.8	-10	-154	-11
	D614G-S704L	1.3	-1.0	-1.6	-1.2	-1.0	-1.0	-1.0	-1.0	-1.3	-1.6	-3.0	1.2	-1.5	-2.7	-1.6	-1.3	-1.7	-1.9	-1.9	-1.9	-1.1	-1.8	-1.5	-1.5	-1.2
	D614G-L452Q/S704L	-1.3	-1.3	-1.9	-1.6	<-7.2	<-1.5	-8.5	-2.8	-32	-4.2	-4.9	-1.5	-48	-2.0	-3.1	-1.8	-1.4	-2.4	-3.0	-2.0	-2.1	-2.4	-2.1	-3.6	-2.2
Compared with BA.2	BA.2-Del69-70	-1.0	-1.5	-1.0	-2.1	-1.0	1.3	-1.0	1.1	-1.0	1.7	1.1	-1.2	1.6	-1.2	-1.0	-1.0	-1.0	<-2.1	-1.0	-1.0	-1.0	-1.5	-1.0	-1.0	1.2
	BA.2-L452M	-1.0	-1.4	-1.0	1.5	-1.0	1.1	-1.0	-1.5	-1.0	-2.2	-2.8	-1.4	<-16	-1.4	-1.3	-1.0	-1.0	1.1	-1.0	-1.0	-1.0	1.2	-1.0	-1.0	1.4
	BA.2-L452R	-1.0	-1.8	-1.0	-5.1	-1.0	-1.2	-1.0	-1.8	-1.0	-5.7	-4.6	-1.1	<-16	-2.6	1.2	-1.0	-1.0	<-2.1	-1.0	-1.0	-1.0	1.3	-1.8	-1.0	<-6.3
	BA.2-L452Q	-1.0	-1.3	-1.0	-1.3	-1.0	1.6	-1.0	1.5	-1.0	-1.8	-1.9	-1.4	<-16	-1.4	-1.6	-1.0	-1.0	<-2.1	-1.0	-1.0	-1.0	-3.2	-1.5	-1.0	-3.5
	BA.2-F486V	-1.0	-8.6	-1.0	<-7.5	1.0	<-9.4	-1.0	<-2182	-1.0	-3.4	1.1	1.1	-1.4	-1.0	-1.7	-1.0	-1.0	-1.2	-1.0	-1.0	-1.0	-5.0	-1.2	-1.0	-3.4
	BA.2-R493Q	>5.0	2.7	-1.0	41.0	>10	22	-1.0	4.6	-1.0	1.1	-1.7	-1.7	-1.7	-1.2	-1.5	-1.0	-1.0	1.6	-1.0	-1.0	-1.0	2.3	1.8	-1.0	76
	BA.2-S704L	-1.0	-1.2	-1.0	-1.1	-1.0	1.5	-1.0	1.2	-1.0	1.9	-1.1	-1.3	-1.1	-1.4	1.1	-1.0	-1.0	1.9	-1.0	-1.0	-1.0	1.2	1.7	-1.0	2.0
	BA.2-F486V/R493Q	-1.0	1.3	-1.0	3.4	-1.0	<-9.4	-1.0	-1694	-1.0	1.5	1.7	1.6	2.2	1.9	1.4	-1.0	-1.0	1.8	-1.0	-1.0	-1.0	1.7	1.1	-1.0	2.7

>10	>3	<-3	<-10	<-100	<-1000

c

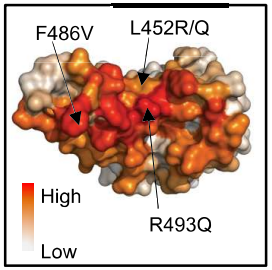

d

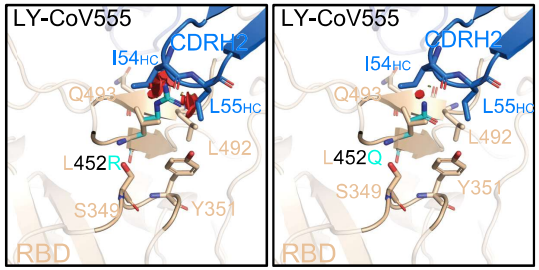

e

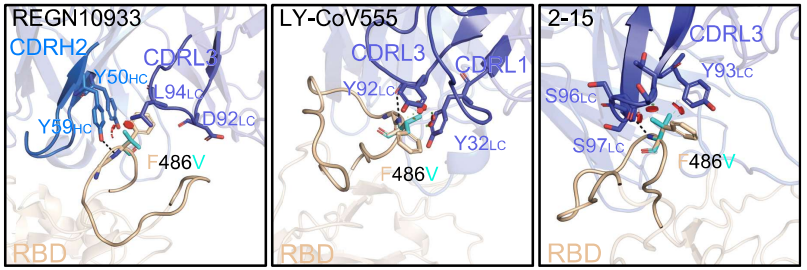

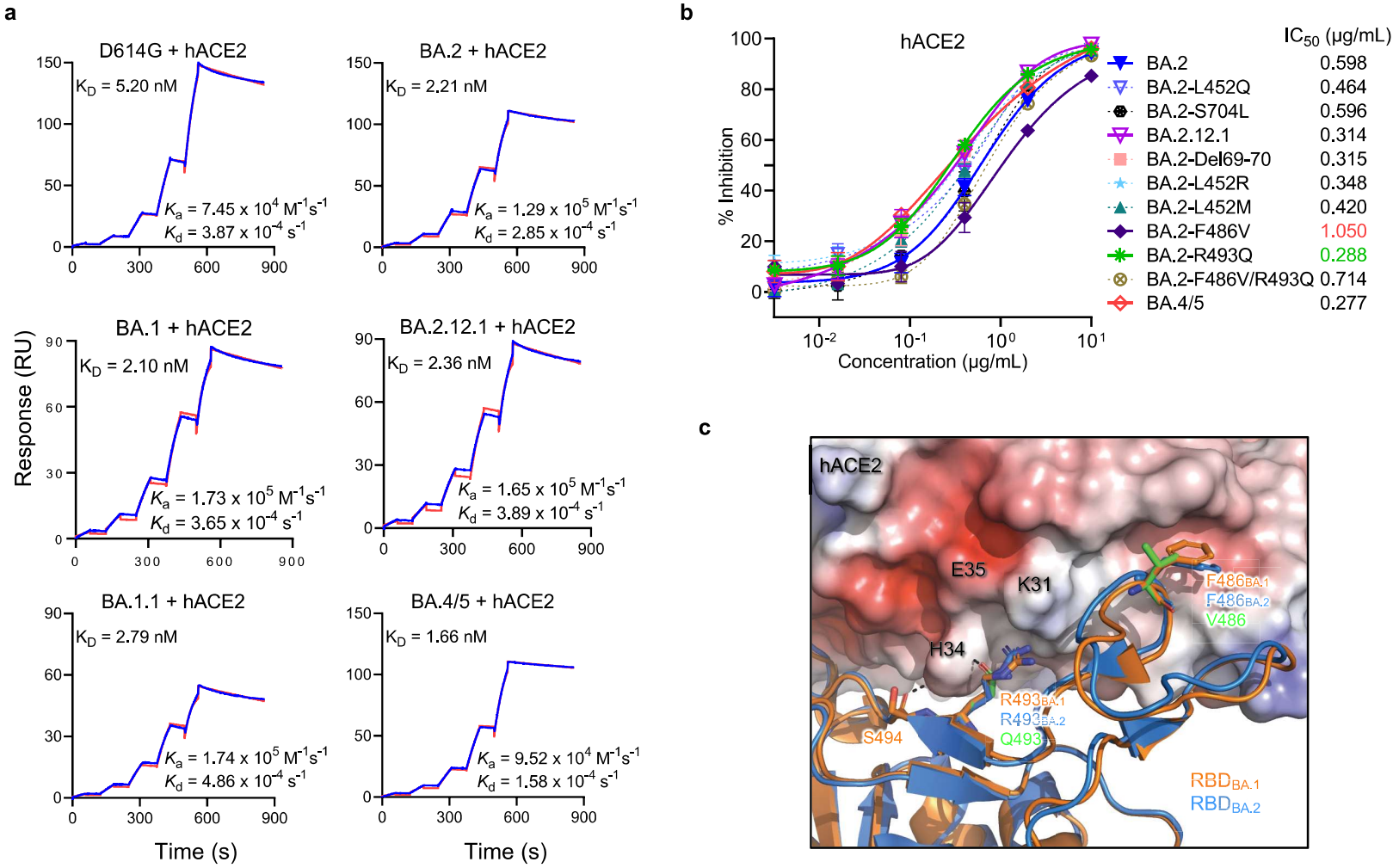
a
D614G + hACE2
K_D = 5.20 nM
K_a = 7.45 x 10^4 M^-1s^-1
K_d = 3.87 x 10^-4 s^-1
BA.2 + hACE2
K_D = 2.21 nM
K_a = 1.29 x 10^5 M^-1s^-1
K_d = 2.85 x 10^-4 s^-1
BA.1 + hACE2
K_D = 2.10 nM
K_a = 1.73 x 10^5 M^-1s^-1
K_d = 3.65 x 10^-4 s^-1
BA.2.12.1 + hACE2
K_D = 2.36 nM
K_a = 1.65 x 10^5 M^-1s^-1
K_d = 3.89 x 10^-4 s^-1
BA.1.1 + hACE2
K_D = 2.79 nM
K_a = 1.74 x 10^5 M^-1s^-1
K_d = 4.86 x 10^-4 s^-1
BA.4/5 + hACE2
K_D = 1.66 nM
K_a = 9.52 x 10^4 M^-1s^-1
K_d = 1.58 x 10^-4 s^-1
Response (RU)
Time (s)
Time (s)
b
hACE2
% Inhibition
Concentration (μg/mL)
IC50 (μg/mL)
BA.2 0.598
BA.2-L452Q 0.464
BA.2-S704L 0.596
BA.2.12.1 0.314
BA.2-Del69-70 0.315
BA.2-L452R 0.348
BA.2-L452M 0.420
BA.2-F486V 1.050
BA.2-R493Q 0.288
BA.2-F486V/R493Q 0.714
BA.4/5 0.277
c
hACE2
E35
K31
H34
S494
F486BA.1
F486BA.2
V486
R493BA.1
R493BA.2
Q493
RBDBA.1
RBDBA.2

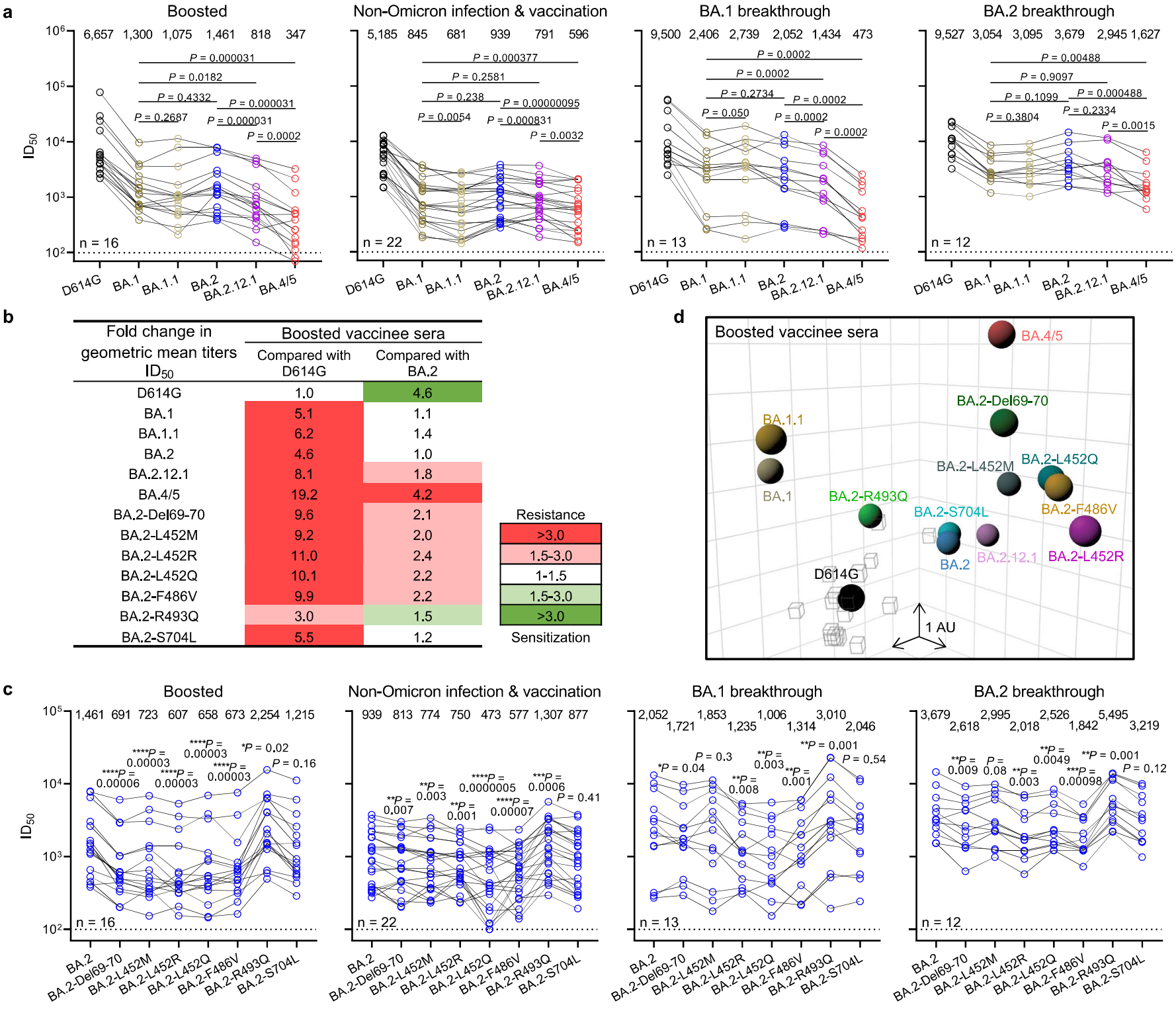
a
Boosted
Non-Omicron infection & vaccination
BA.1 breakthrough
BA.2 breakthrough
ID50
n = 16
n = 22
n = 13
n = 12
D614G
BA.1
BA.1.1
BA.2
BA.2.12.1
BA.4/5
b
Fold change in geometric mean titers ID50
Boosted vaccinee sera
Compared with D614G
Compared with BA.2
D614G 1.0 4.6
BA.1 5.1 1.1
BA.1.1 6.2 1.4
BA.2 4.6 1.0
BA.2.12.1 8.1 1.8
BA.4/5 19.2 4.2
BA.2-Del69-70 9.6 2.1
BA.2-L452M 9.2 2.0
BA.2-L452R 11.0 2.4
BA.2-L452Q 10.1 2.2
BA.2-F486V 9.9 2.2
BA.2-R493Q 3.0 1.5
BA.2-S704L 5.5 1.2
Resistance
>3.0
1.5-3.0
1-1.5
1.5-3.0
>3.0
Sensitization
d
Boosted vaccinee sera
BA.4/5
BA.2-Del69-70
BA.1.1
BA.2-L452M
BA.2-L452Q
BA.1
BA.2-R493Q
BA.2-S704L
BA.2-F486V
BA.2
BA.2.12.1
BA.2-L452R
D614G
1 AU
c
Boosted
Non-Omicron infection & vaccination
BA.1 breakthrough
BA.2 breakthrough
ID50
n = 16
n = 22
n = 13
n = 12
BA.2
BA.2-Del69-70
BA.2-L452M
BA.2-L452R
BA.2-L452Q
BA.2-F486V
BA.2-R493Q
BA.2-S704L

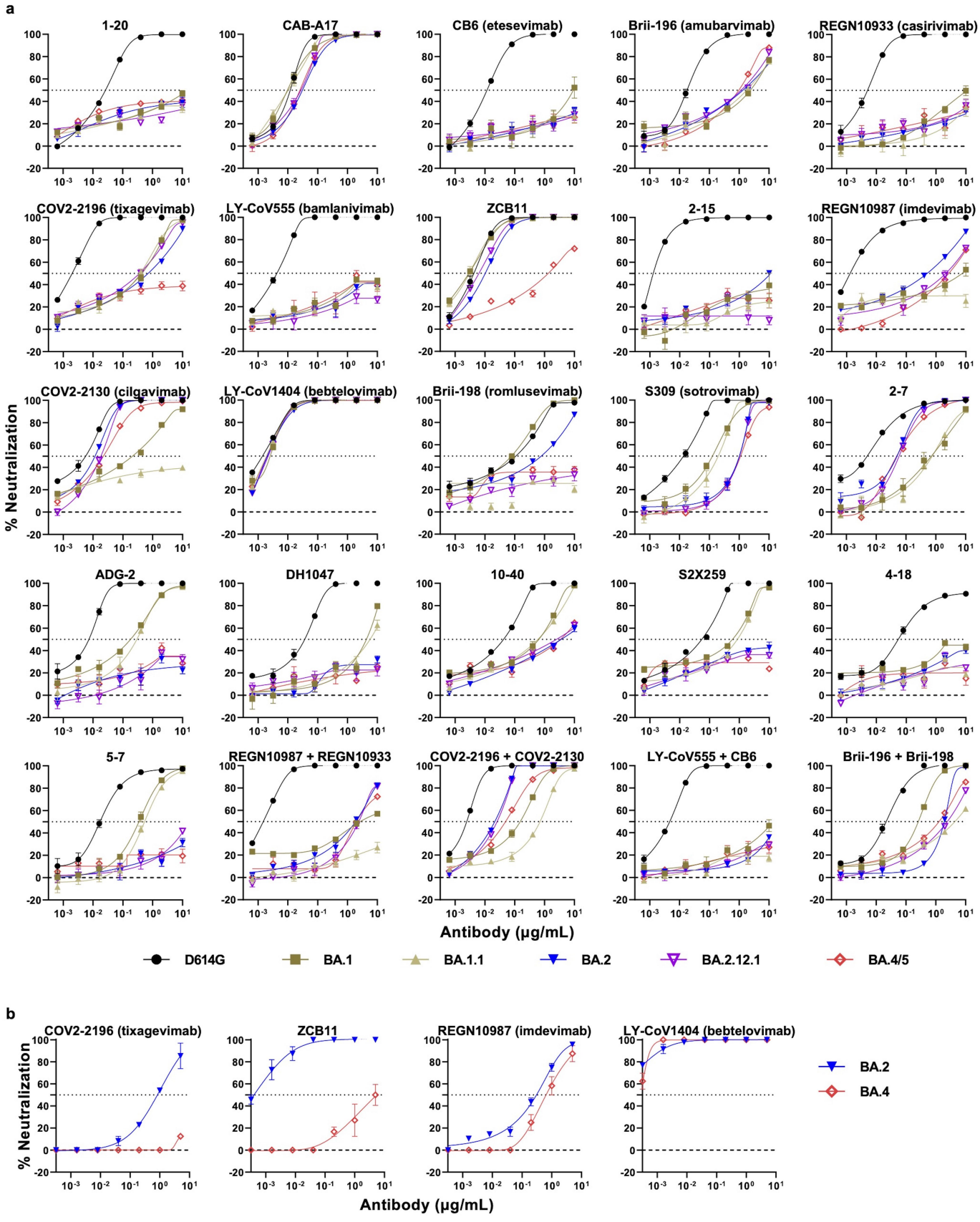

Extended Data Fig. 1

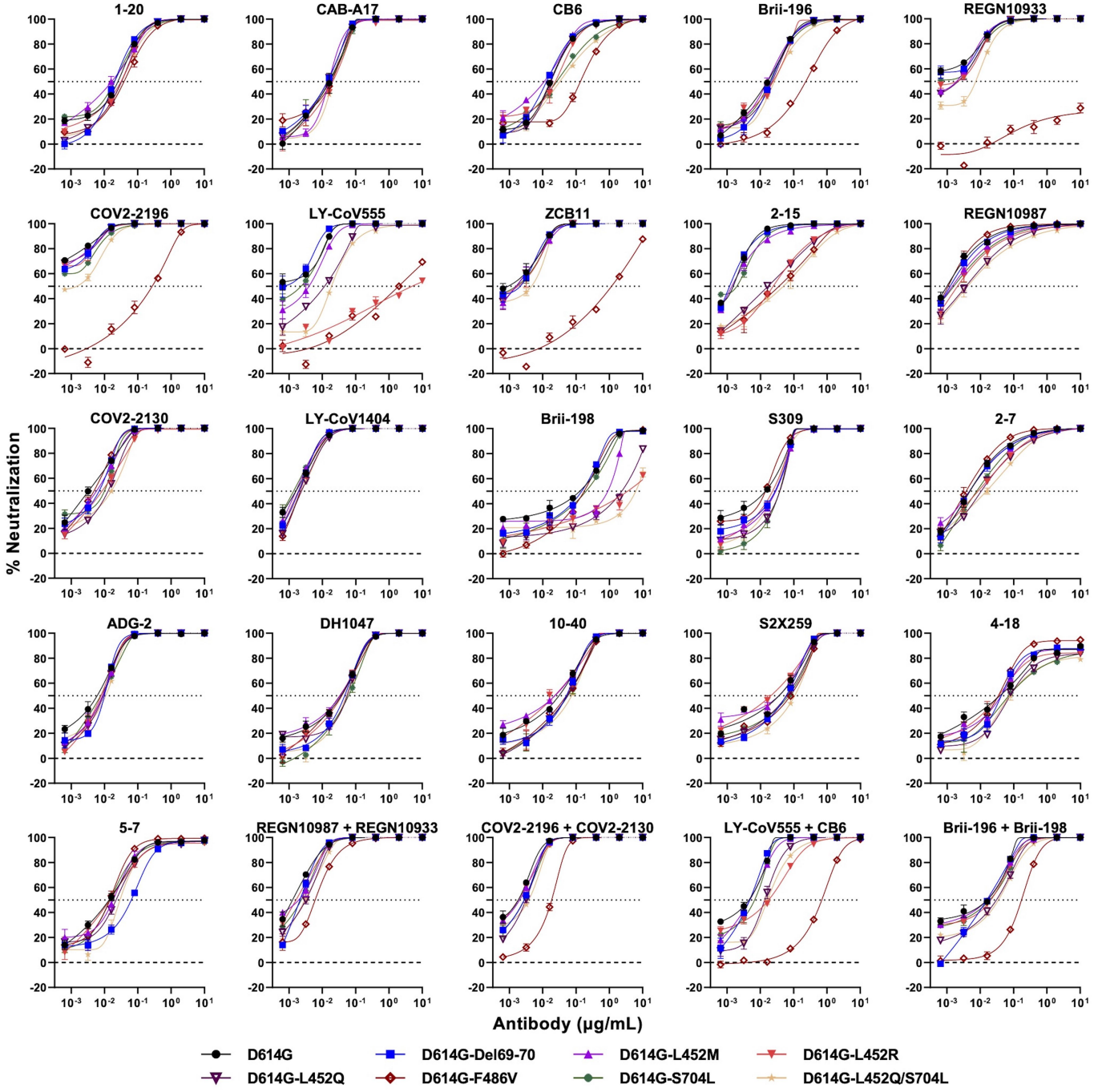

Extended Data Fig. 2

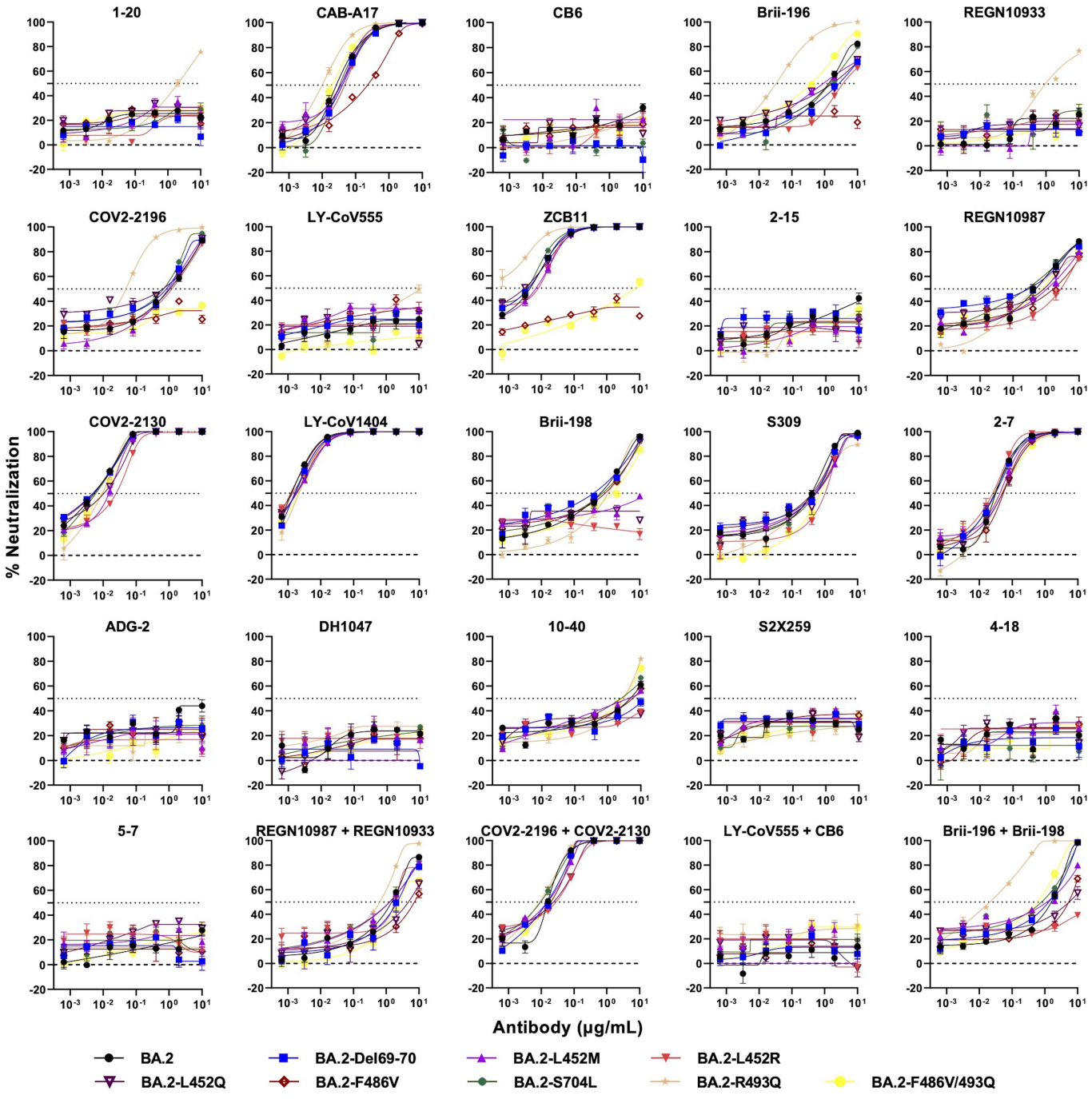

Extended Data Fig. 3

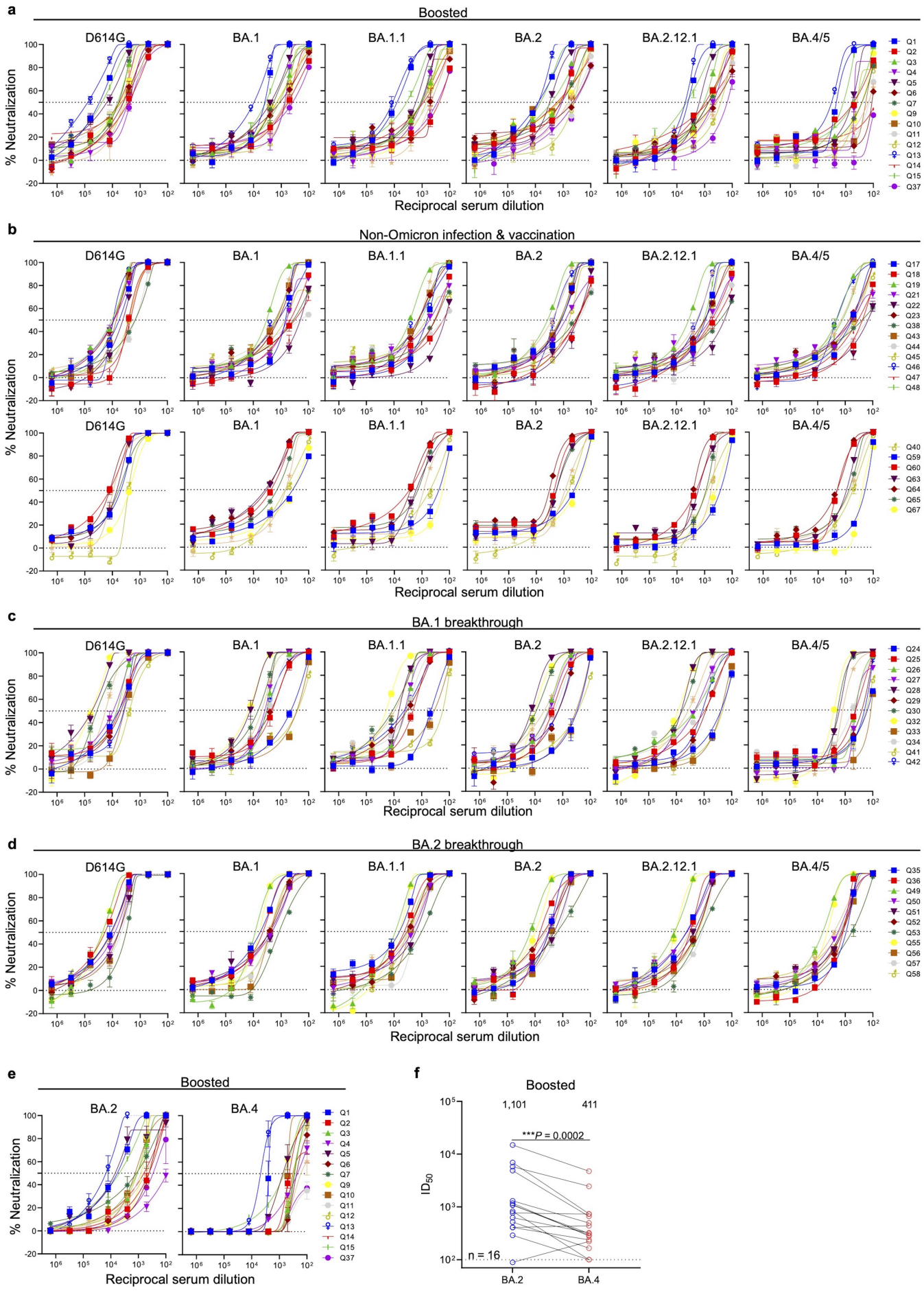

Extended Data Fig. 4

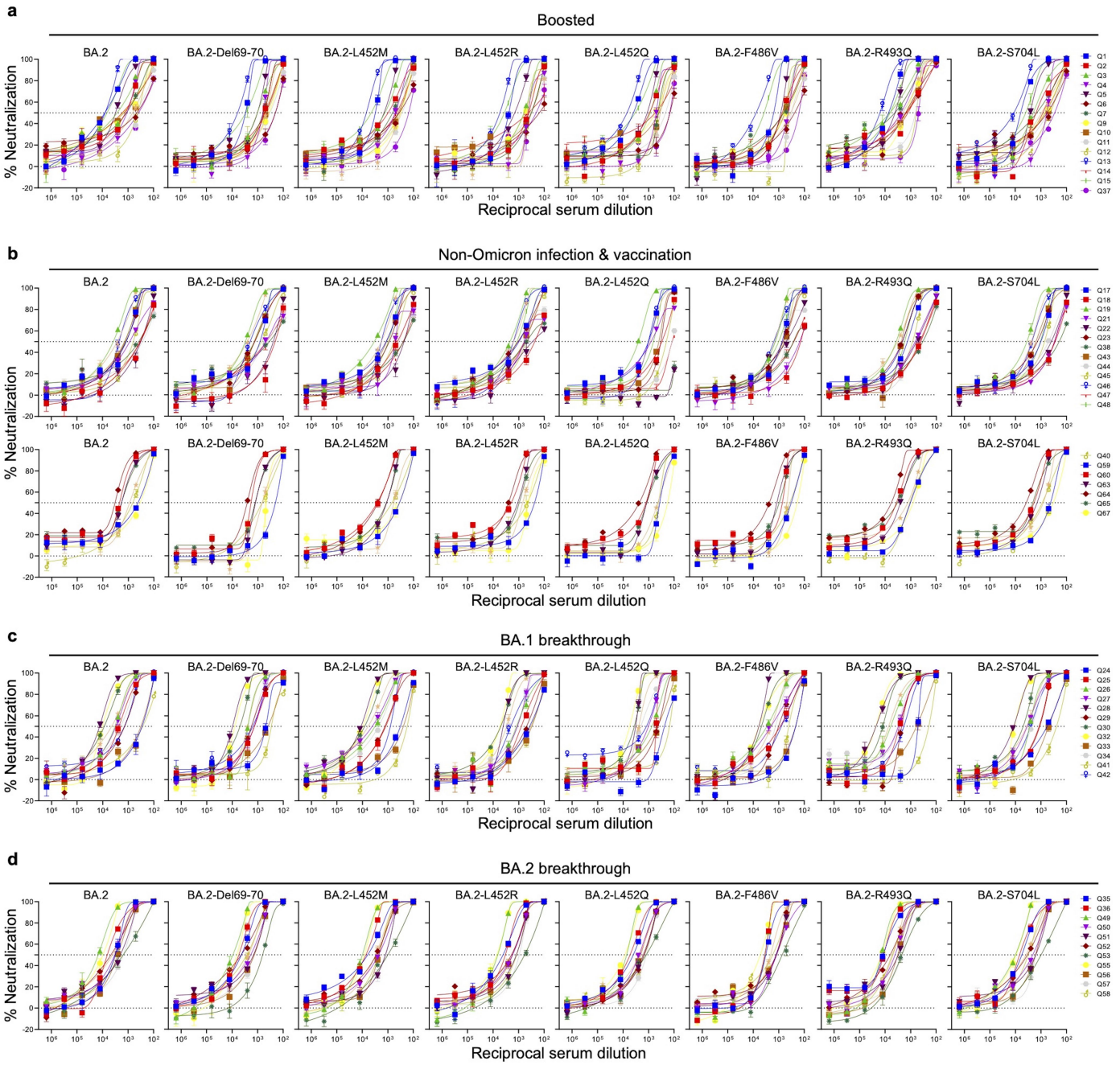

Extended Data Fig. 5

a

IC50 (μg/mL)	RBD mAbs																			NTD mAbs		Combination			
	Class 1				Class 2					Class 3						Class 4									
	1-20	CAB-A17	CB6	Brii-196	REGN 10933	COV2-2196	LY-CoV555	ZCB11	2-15	REGN 10987	COV2-2130	LY-CoV 1404	Brii-198	S309	2-7	ADG-2	DH1047	10-40	S2X259	4-18	5-7	REGN 10987 + REGN 10933	COV2-2196 + COV2-2130	LY-CoV555 + CB6	Brii-196 + Brii-198
D614G	0.027	0.012	0.012	0.018	0.005	0.002	0.004	0.004	0.001	0.001	0.006	0.001	0.110	0.014	0.005	0.007	0.037	0.042	0.055	0.054	0.017	0.001	0.002	0.005	0.022
BA.1	>10	0.010	9.253	2.385	>10	0.432	>10	0.003	>10	7.586	0.209	0.003	0.078	0.127	0.716	0.181	4.322	0.644	0.590	>10	0.347	2.951	0.154	>10	0.260
BA.1.1	>10	0.010	>10	1.792	>10	0.385	>10	0.003	>10	>10	>10	0.002	>10	0.200	0.763	0.295	5.723	0.600	0.859	>10	0.534	>10	0.708	>10	4.394
BA.2	>10	0.031	>10	1.346	>10	0.704	>10	0.010	>10	0.505	0.012	0.002	0.782	1.019	0.050	>10	>10	3.642	>10	>10	>10	1.882	0.021	>10	1.907
BA.2.12.1	>10	0.027	>10	1.171	>10	0.361	>10	0.006	>10	2.125	0.018	0.002	>10	1.035	0.059	>10	>10	2.519	>10	>10	>10	2.400	0.026	>10	1.936
BA.4/5	>10	0.025	>10	0.978	>10	>10	>10	1.351	>10	2.682	0.022	0.002	>10	1.120	0.049	>10	>10	3.404	>10	>10	>10	1.998	0.049	>10	2.445

<0.01	<0.1	<1	<10	>10

b

IC50 (μg/mL)	RBD mAbs			
	Class 2		Class 3	
	COV2-2196	ZCB11	REGN 10987	LY-CoV1404
BA.2	0.8287	0.0004	0.3057	<0.001
BA.4	>5	>5	0.6418	<0.001

<0.01	<0.1	<1	<5	>5

Extended Data Table 1

a

IC50 (μg/mL)	RBD mAbs																			NTD mAbs		Combination			
	Class 1				Class 2					Class 3						Class 4									
	1-20	CAB-A17	CB6	Brii-196	REGN 10933	COV2-2196	LY-CoV 555	ZCB11	2-15	REGN 10987	COV2-2130	LY-CoV 1404	Brii-198	S309	2-7	ADG-2	DH1047	10-40	S2X259	4-18	5-7	REGN 10987 + REGN 10933	COV2-2196 + COV2-2130	LY-CoV555 + CB6	Brii-196 + Brii-198
D614G	0.026	0.016	0.017	0.016	<0.001	<0.001	0.002	0.002	0.002	0.001	0.003	0.002	0.129	0.014	0.005	0.006	0.037	0.031	0.036	0.038	0.014	0.001	0.002	0.005	0.016
D614G-Del69-70	0.020	0.014	0.013	0.021	<0.001	<0.001	0.001	0.002	0.001	0.001	0.007	0.002	0.148	0.028	0.005	0.010	0.047	0.051	0.059	0.042	0.064	0.002	0.003	0.005	0.016
D614G-L452M	0.017	0.016	0.011	0.016	0.002	<0.001	0.004	0.002	0.001	0.001	0.006	0.002	0.892	0.029	0.005	0.009	0.034	0.023	0.036	0.042	0.018	0.002	0.002	0.005	0.016
D614G-L452R	0.032	0.020	0.024	0.024	0.002	<0.001	5.018	0.002	0.024	0.002	0.009	0.002	3.526	0.023	0.009	0.008	0.039	0.023	0.020	0.035	0.014	0.002	0.002	0.018	0.021
D614G-L452Q	0.033	0.014	0.018	0.023	0.002	<0.001	0.012	0.002	0.017	0.004	0.013	0.002	2.346	0.038	0.011	0.009	0.056	0.055	0.061	0.078	0.022	0.003	0.003	0.013	0.031
D614G-F486V	0.039	0.019	0.135	0.231	>10	0.272	1.961	1.174	0.036	0.001	0.005	0.002	0.175	0.014	0.004	0.009	0.033	0.051	0.079	0.034	0.014	0.006	0.019	0.701	0.174
D614G-S704L	0.020	0.017	0.026	0.019	<0.001	<0.001	0.002	0.002	0.002	0.002	0.010	0.001	0.199	0.038	0.008	0.008	0.061	0.057	0.069	0.071	0.015	0.002	0.003	0.007	0.019
D614G-L452Q/S704L	0.033	0.020	0.032	0.026	0.007	0.001	0.019	0.005	0.049	0.004	0.016	0.002	6.166	0.028	0.015	0.011	0.052	0.074	0.106	0.076	0.029	0.003	0.004	0.016	0.035

b

IC50 (μg/mL)	RBD mAbs																			NTD mAbs		Combination			
	Class 1				Class 2					Class 3						Class 4									
	1-20	CAB-A17	CB6	Brii-196	REGN 10933	COV2-2196	LY-CoV 555	ZCB11	2-15	REGN 10987	COV2-2130	LY-CoV 1404	Brii-198	S309	2-7	ADG-2	DH1047	10-40	S2X259	4-18	5-7	REGN 10987 + REGN 10933	COV2-2196 + COV2-2130	LY-CoV555 + CB6	Brii-196 + Brii-198
BA.2	>10	0.027	>10	1.329	>10	1.060	>10	0.005	>10	0.495	0.005	0.001	0.642	0.393	0.032	>10	>10	4.824	>10	>10	>10	1.475	0.016	>10	1.592
BA.2-Del69-70	>10	0.040	>10	2.726	>10	0.835	>10	0.004	>10	0.298	0.005	0.002	0.394	0.469	0.031	>10	>10	>10	>10	>10	>10	2.178	0.015	>10	1.320
BA.2-L452M	>10	0.036	>10	0.907	>10	0.970	>10	0.007	>10	1.081	0.015	0.002	>10	0.557	0.042	>10	>10	4.246	>10	>10	>10	1.276	0.015	>10	1.163
BA.2-L452R	>10	0.047	>10	6.815	>10	1.228	>10	0.008	>10	2.832	0.025	0.001	>10	1.022	0.026	>10	>10	>10	>10	>10	>10	1.864	0.028	>10	>10
BA.2-L452Q	>10	0.036	>10	1.717	>10	0.655	>10	0.003	>10	0.872	0.010	0.002	>10	0.535	0.051	>10	>10	>10	>10	>10	>10	4.793	0.024	>10	5.525
BA.2-F486V	>10	0.229	>10	>10	>10	>10	>10	>10	>10	1.681	0.005	0.001	0.887	0.412	0.054	>10	>10	5.759	>10	>10	>10	7.366	0.020	>10	5.377
BA.2-R493Q	2.020	0.010	>10	0.033	0.960	0.049	>10	<0.001	>10	0.454	0.009	0.002	1.089	0.485	0.049	>10	>10	3.008	>10	>10	>10	0.641	0.009	>10	0.021
BA.2-S704L	>10	0.033	>10	1.464	>10	0.686	>10	0.004	>10	0.262	0.006	0.002	0.735	0.539	0.029	>10	>10	2.537	>10	>10	>10	1.262	0.010	>10	0.800
BA.2-F486V/R493Q	>10	0.020	>10	0.394	>10	>10	>10	7.766	>10	0.757	0.009	0.002	1.414	0.754	0.044	>10	>10	2.751	>10	>10	>10	2.498	0.017	>10	0.586

<0.01	<0.1	<1	<10	>10

Extended Data Table 2

Mutation	Count in BA.1	Frequency in BA.1	Count in BA.2	Frequency in BA.2	Count in other variants	Frequency in other variants
F486V	23	2.17E-06	134	1.26E-05	898	8.48E-05
Del486	193	1.82E-05	549	5.18E-05	760	7.17E-05
F486L	37	3.49E-06	10	9.44E-07	155	1.46E-05
F486S	61	5.76E-06	10	9.44E-07	142	1.34E-05
F486I	5	4.72E-07	2	1.89E-07	34	3.21E-06
F486Y	12	1.13E-06	2	1.89E-07	20	1.89E-06
F486W	8	7.55E-07	1	9.44E-08	10	9.44E-07
F486T	5	4.72E-07	0	0	5	4.72E-07
F486E	2	1.89E-07	0	0	3	2.83E-07
F486N	2	1.89E-07	0	0	3	2.83E-07
F486H	2	1.89E-07	0	0	2	1.89E-07
F486P	2	1.89E-07	0	0	2	1.89E-07
F486R	1	9.44E-08	0	0	2	1.89E-07
F486C	0	0	0	0	1	9.44E-08
F486G	1	9.44E-08	0	0	1	9.44E-08
F486M	0	0	0	0	1	9.44E-08
F486Q	0	0	1	9.44E-08	1	9.44E-08

Extended Data Table 3

Sample ID	Vaccine type and infected strain	Days post-vaccination or *infection (after last exposure)	Documented COVID-19	Age	Gender
Boosted					
Q1	mRNA-1273/mRNA-1273/mRNA-1273	29	No	66	Female
Q2	BNT162b2/BNT162b2/BNT162b2	30	No	68	Male
Q3	BNT162b2/BNT162b2/BNT162b2	14	No	64	Female
Q4	BNT162b2/BNT162b2/BNT162b2	34	No	55	Male
Q5	BNT162b2/BNT162b2/BNT162b2	34	No	45	Male
Q6	BNT162b2/BNT162b2/BNT162b2	15	No	50	Female
Q7	BNT162b2/BNT162b2/BNT162b2	15	No	48	Female
Q8	BNT162b2/BNT162b2/BNT162b2	29	No	71	Male
Q9	BNT162b2/BNT162b2/BNT162b2	90	No	59	Male
Q10	BNT162b2/BNT162b2/BNT162b2	33	No	45	Male
Q11	BNT162b2/BNT162b2/BNT162b2	87	No	66	Female
Q12	BNT162b2/BNT162b2/BNT162b2	84	No	26	Male
Q13	mRNA-1273/mRNA-1273/mRNA-1273	23	No	28	Female
Q14	BNT162b2/BNT162b2/BNT162b2	14	No	78	Male
Q15	BNT162b2/BNT162b2/mRNA-1273	32	No	39	Male
Q37	BNT162b2/BNT162b2/BNT162b2	20	No	Unknown	Female
Non-Omicron infection & vaccination					
Q17	R.1/mRNA-1273/mRNA-1273	7	Yes	34	Female
Q18	R.1/mRNA-1273/mRNA-1273	28	Yes	52	Male
Q19	R.1/mRNA-1273/mRNA-1273	21	Yes	67	Female
Q21	R.1/mRNA-1273/mRNA-1273	>28	Yes	57	Female
Q22	BNT162b2/B.1.526	*89	Yes	42	Male
Q23	BNT162b2/B.1.526	*82	Yes	32	Male
Q38	BNT162b2/B.1.1.7	*59	Yes	22	Female
Q39	BNT162b2/B.1.1.7	*213	Yes	66	Male
Q40	BNT162b2/B.1.617.2	*31	Yes	50	Female
Q43	BNT162b2/BNT162b2/B.1.526	*62	Yes	30	Male
Q44	WA1/mRNA-1273/mRNA-1273	114	Yes	49	Female
Q45	WA1/BNT162b2/BNT162b2	57	Yes	35	Female
Q46	WA1/BNT162b2/BNT162b2	46	Yes	30	Female
Q47	WA1/BNT162b2/BNT162b2	57	Yes	32	Female
Q48	WA1/BNT162b2/BNT162b2	50	Yes	64	Female
Q59	BNT162b2/BNT162b2/B.1.617.2	*35	Yes	58	Female
Q60	B.1.617.2/BNT162b2/BNT162b2	40	Yes	61	Male
Q63	BNT162b2/BNT162b2/B.1.617.2	*30	Yes	40	Female
Q64	mRNA-1273/mRNA-1273/B.1.617.2	*66	Yes	29	Male
Q65	BNT162b2/BNT162b2/B.1.617.2	*62	Yes	33	Female
Q66	BNT162b2/BNT162b2/B.1.617.2	*60	Yes	42	Female
Q67	BNT162b2/BNT162b2/B.1.617.2	*73	Yes	37	Male
BA.1 breakthrough					
Q24	BNT162b2/BNT162b2/BA.1	*14	Yes	Unknown	Unknown
Q25	BNT162b2/BNT162b2/BA.1	*14	Yes	Unknown	Unknown
Q26	mRNA-1273/mRNA-1273/BA.1	*35	Yes	Unknown	Unknown
Q27	BNT162b2/BNT162b2/BNT162b2/BA.1	*135	Yes	78	Male
Q28	BNT162b2/BNT162b2/BNT162b2/BA.1	*14	Yes	Unknown	Unknown
Q29	BNT162b2/BNT162b2/BNT162b2/BA.1	*14	Yes	Unknown	Unknown
Q30	BNT162b2/BNT162b2/BNT162b2/BA.1	*14	Yes	Unknown	Unknown
Q31	BNT162b2/BNT162b2/BNT162b2/BA.1	*41	Yes	48	Male
Q32	BNT162b2/BNT162b2/BNT162b2/BA.1	*26	Yes	38	Female
Q33	BNT162b2/BNT162b2/B.1.617.2/BNT162b2/BA.1	*19	Yes	35	Female
Q34	BNT162b2/BNT162b2/mRNA-1273/mRNA-1273/BA.1	*67	Yes	40	Male
Q41	WA1/BNT162b2/BA.1	*21	Yes	52	Male
Q42	WA1/BNT162b2/BA.1	*44	Yes	37	Intersex
BA.2 breakthrough					
Q35	BNT162b2/BNT162b2/BA.2	*14	Yes	50	Female
Q36	BNT162b2/BNT162b2/BNT162b2/Ad26.COV2.S/BA.2	*22	Yes	69	Male
Q49	BNT162b2/BNT162b2/mRNA-1273/BA.2	*16	Yes	32	Male
Q50	mRNA-1273/mRNA-1273/mRNA-1273/BA.2	*14	Yes	34	Male
Q51	BNT162b2/BNT162b2/mRNA-1273/BA.2	*19	Yes	33	Female
Q52	BNT162b2/BNT162b2/mRNA-1273/BA.2	*18	Yes	29	Female
Q53	BNT162b2/BNT162b2/BNT162b2/BA.2	*25	Yes	34	Male
Q54	BNT162b2/BNT162b2/BNT162b2/BA.2	*36	Yes	37	Female
Q55	BNT162b2/BNT162b2/mRNA-1273/BA.2	*18	Yes	41	Female
Q56	mRNA-1273/mRNA-1273/mRNA-1273/BA.2	*21	Yes	36	Female
Q57	BNT162b2/BNT162b2/mRNA-1273/BA.2	*32	Yes	28	Male
Q58	BNT162b2/BNT162b2/mRNA-1273/BA.2	*23	Yes	33	Female

Extended Data Table 4

nature portfolio

Corresponding author(s): David D. Ho

Last updated by author(s): Jun 26, 2022

Reporting Summary

Nature Portfolio wishes to improve the reproducibility of the work that we publish. This form provides structure for consistency and transparency in reporting. For further information on Nature Portfolio policies, see our Editorial Policies and the Editorial Policy Checklist.

Statistics

For all statistical analyses, confirm that the following items are present in the figure legend, table legend, main text, or Methods section.

n/a	Confirmed	
☐	☒	The exact sample size (*n*) for each experimental group/condition, given as a discrete number and unit of measurement
☐	☒	A statement on whether measurements were taken from distinct samples or whether the same sample was measured repeatedly
☐	☒	The statistical test(s) used AND whether they are one- or two-sided *Only common tests should be described solely by name; describe more complex techniques in the Methods section.*
☒	☐	A description of all covariates tested
☒	☐	A description of any assumptions or corrections, such as tests of normality and adjustment for multiple comparisons
☐	☒	A full description of the statistical parameters including central tendency (e.g. means) or other basic estimates (e.g. regression coefficient) AND variation (e.g. standard deviation) or associated estimates of uncertainty (e.g. confidence intervals)
☐	☒	For null hypothesis testing, the test statistic (e.g. *F*, *t*, *r*) with confidence intervals, effect sizes, degrees of freedom and *P* value noted *Give P values as exact values whenever suitable.*
☒	☐	For Bayesian analysis, information on the choice of priors and Markov chain Monte Carlo settings
☒	☐	For hierarchical and complex designs, identification of the appropriate level for tests and full reporting of outcomes
☒	☐	Estimates of effect sizes (e.g. Cohen's *d*, Pearson's *r*), indicating how they were calculated

Our web collection on statistics for biologists contains articles on many of the points above.

Software and code

Policy information about availability of computer code

Data collection	SoftMax Pro 7.0.2 (Molecular Devices, LLC) was used to measure luminescence in the pseudovirus neutralization assays. Biacore T200 biosensor (Cytiva) was used to measure the spike-ACE2 binding affinity.
Data analysis	GraphPad Prism (version 9.2) was used for data visualization and for statistical tests. PISA was used for indetifying antibody-spike interface residues. PyMOL v.2.3.2 was used to perform mutagenesis and to generate structural plots. SPR data were fitted with Biacore T200 Evaluation Software (Version 1.0). The Racmacs package (https://acorg.github.io/Racmacs/, version 1.1.4) was used to generate the antigenic cartography.

For manuscripts utilizing custom algorithms or software that are central to the research but not yet described in published literature, software must be made available to editors and reviewers. We strongly encourage code deposition in a community repository (e.g. GitHub). See the Nature Portfolio guidelines for submitting code & software for further information.

Data

Policy information about availability of data

All manuscripts must include a data availability statement. This statement should provide the following information, where applicable:

- Accession codes, unique identifiers, or web links for publicly available datasets
- A description of any restrictions on data availability
- For clinical datasets or third party data, please ensure that the statement adheres to our policy

All experimental data are provided in the manuscript. Materials used in this study will be available under an appropriated Materials Transfer Agreement. An interactive antigenic map based on the neutralization data of boosted vaccinee sera (Figure 4b) is available online (https://figshare.com/articles/media/OmicronAntigenicMap/19854046). Sequences for Omicron prevalence analysis were downloaded from GISAID (https://www.gisaid.org/). The structures used for analysis in this study are available from PDB under IDs 6ZGE, 7L5B, 6XDG, 7U0N, 7UB0 and 7KMG.

Human research participants

Policy information about studies involving human research participants and Sex and Gender in Research.

Reporting on sex and gender	Sex and gender of the participants in this study are described in detail in the Extended Data Table 2: 30/63 female, 26/63 male, 1/63 intersex, 6/63 unknown sex; 7/63 unknown age, 56/63 22-78 years old.
Population characteristics	A total of 63 individuals were enrolled in this study. Population characteristics for the sera utilized in the pseudovirus neutralization assays are described in the Extended Data Table 2.
Recruitment	Participants volunteered and were enrolled in an observational cohort study at Columbia University Irving Medical Center or at the Hackensack Meridian Center for Discovery and Innovation (CDI) to study the immunological responses to SARS-CoV-2 in individuals who had received COVID-19 vaccines. Self-selection biases may have affected the demographics of the enrolled population, but are not expected to have impacted the results of this study. High titer samples were specifically chosen so that fold-changes in titer could be better determined.
Ethics oversight	All collections were conducted under protocols reviewed and approved by the Institutional Review Board of Columbia University or or the Hackensack Meridian Center for Discovery and Innovation. All of the participants provided written informed consent.

Note that full information on the approval of the study protocol must also be provided in the manuscript.

Field-specific reporting

Please select the one below that is the best fit for your research. If you are not sure, read the appropriate sections before making your selection.

☒ Life sciences ☐ Behavioural & social sciences ☐ Ecological, evolutionary & environmental sciences

For a reference copy of the document with all sections, see nature.com/documents/nr-reporting-summary-flat.pdf

Life sciences study design

All studies must disclose on these points even when the disclosure is negative.

Sample size	No statistical methods were used to predetermine sample size. We used analogous sample sizes as in previous work (e.g. Wang et al 2021, Nature; Liu et al 2022, Nature; Iketani et al 2022, Nature), which we had previously determined to be sufficient sample sizes for comparisons between groups for these experiments. The human research participants (n=63) in this study were characterized in 4 groups, including Boosted (n=16), Non-Omicron infection & vaccination (n=22), BA.1 breakthrough (n=13) and BA.2 breakthrough (n=12).
Data exclusions	No data were excluded.
Replication	The antibody neutralization assays, the serum neutralization assays, the huACE2 inhibition assays were repeated twice independently in technical triplicate with similar results. SPR assays were repeated twice independently with similar results. The results that are shown are representative. All replicates for the neutralization assays and SPR assays are reproducible and successful.
Randomization	As this is an observational study, randomization is not relevant.
Blinding	As this is an observational study, investigators were not blinded.

Reporting for specific materials, systems and methods

We require information from authors about some types of materials, experimental systems and methods used in many studies. Here, indicate whether each material, system or method listed is relevant to your study. If you are not sure if a list item applies to your research, read the appropriate section before selecting a response.

Materials & experimental systems

n/a	Involved in the study
☐	☒ Antibodies
☐	☒ Eukaryotic cell lines
☒	☐ Palaeontology and archaeology
☒	☐ Animals and other organisms
☒	☐ Clinical data
☒	☐ Dual use research of concern

Methods

n/a	Involved in the study
☒	☐ ChIP-seq
☒	☐ Flow cytometry
☒	☐ MRI-based neuroimaging

Antibodies

Antibodies used	All of the antibodies used in this study were produced in our laboratory or provided by other laboratories or companies. 1-20, CAB-A17, LY-CoV555, 2-15, S309, 2-7, LY-CoV1404, ADG-2, DH1047, 10-40, S2X259, 4-18, and 5-7 were expressed and purified in-house as described previously in Liu et al 2020, Nature and in the Methods section of this manuscript. REGN10933, COV2-2196, REGN10987, and COV2-2130 were produced and provided by Regeneron Pharmaceuticals, Brii-196 and Brii-198 were produced and provided by Brii Biosciences, CB6 was produced and provided by Baoshan Zhang and Peter Kwong (NIAID), and ZCB11 was produced and provided by Zhiwei Chen (HKU).
Validation	All of the antibodies have been validated in previous studies by neutralization of SARS-CoV-2. Specifically, 1-20, CB6, Brii-196, REGN10933, COV2-2196, LY-CoV555, 2-15, REGN10987, COV2-2130, LY-CoV1404, Brii-198, S309, 2-7, ADG-2, 10-40, S2X259, 4-18, and 5-7 were tested in Liu et al 2022, Nature, Iketani et al 2022, Nature, or Liu et al 2022, Science Translational Medicine. CAB-A17 and ZCB11 were newly produced and tested prior to use in this study and confirmed to have similar results as that of the original publications (Sheward et al 2022, BioRxiv and Zhou et al 2022, BioRxiv, respectively).

Eukaryotic cell lines

Policy information about cell lines and Sex and Gender in Research

Cell line source(s)	HEK293T cells were obtained from ATCC (Cat #CRL-3216). Vero-E6 cells were obtained from ATCC (Cat #CRL-1586). Expi293 cells were obtained from Thermo Fisher (Cat #A14527).
Authentication	Cells were purchased from authenticated vendors and morphology was confirmed visually before use.
Mycoplasma contamination	cell lines tested mycoplasma negative.
Commonly misidentified lines (See ICLAC register)	No commonly misidentified cell lines were used in this study.